UC San Diego
UC San Diego Previously Published Works

Title

Hook3 is a scaffold for the opposite-polarity microtubule-based motors cytoplasmic dynein-1 and KIF1C

Permalink

Journal

ISSN

Authors

Kendrick, Agnieszka A
Dickey, Andrea M
Redwine, William B
et al.

Publication Date

DOI

Peer reviewed

ARTICLE

Hook3 is a scaffold for the opposite-polarity microtubule-based motors cytoplasmic dynein-1 and KIF1C

Agnieszka A. Kendrick[1], Andrea M. Dickey[1]*, William B. Redwine[1,2]*, Phuoc Tien Tran[1], Laura Pontano Vaites[2], Monika Dzieciatkowska[3], J. Wade Harper[2], and Samara L. Reck-Peterson[1,4,5]

The unidirectional and opposite-polarity microtubule-based motors, dynein and kinesin, drive long-distance intracellular cargo transport. Cellular observations suggest that opposite-polarity motors may be coupled. We recently identified an interaction between the cytoplasmic dynein-1 activating adaptor Hook3 and the kinesin-3 KIF1C. Here, using in vitro reconstitutions with purified components, we show that KIF1C and dynein/dynactin can exist in a complex scaffolded by Hook3. Full-length Hook3 binds to and activates dynein/dynactin motility. Hook3 also binds to a short region in the "tail" of KIF1C, but unlike dynein/dynactin, this interaction does not activate KIF1C. Hook3 scaffolding allows dynein to transport KIF1C toward the microtubule minus end, and KIF1C to transport dynein toward the microtubule plus end. In cells, KIF1C can recruit Hook3 to the cell periphery, although the cellular role of the complex containing both motors remains unknown. We propose that Hook3's ability to scaffold dynein/dynactin and KIF1C may regulate bidirectional motility, promote motor recycling, or sequester the pool of available dynein/dynactin activating adaptors.

Introduction

In many eukaryotic organisms, microtubules and the motors that move on them (kinesins and dynein) power the long-distance transport of intracellular cargos. Microtubules are polar structures with their "minus ends" typically located near microtubule organizing centers. Cytoplasmic dynein-1 ("dynein" here) moves cargos toward the microtubule minus end, while kinesins that transport cargos over long distances, such as those in the kinesin-1, -2, and -3 families, move cargos toward the microtubule plus end (Vale, 2003). The cargos of these motors include organelles, other membrane-bound compartments, and large RNA and protein complexes (Hirokawa and Noda, 2008; Reck-Peterson et al., 2018).

In many cases, these cargos can be observed rapidly switching directions. For example, in filamentous fungi, endosomes move bidirectionally along microtubules (Wedlich-Söldner et al., 2002; Abenza et al., 2009; Egan et al., 2012) and also drive the bidirectional motility of hitchhiking cargos

such as peroxisomes, lipid droplets, endoplasmic reticulum, and ribonucleoprotein complexes (Baumann et al., 2012; Guimaraes et al., 2015; Salogiannis et al., 2016). In human cells, examples of cargos that move bidirectionally on microtubules include lysosomes (Hendricks et al., 2010), secretory vesicles (Barkus et al., 2008; Schlager et al., 2010), autophagosomes (Maday et al., 2012), and protein aggregates (Kamal et al., 2000; Encalada et al., 2011). Purified cargos, such as pigment granules (Rogers et al., 1997) and neuronal transport vesicles (Hendricks et al., 2010), exhibit bidirectional motility along microtubules in vitro. Together, these data suggest that opposite-polarity motors are present on the same cargos in many organisms and for many cargo types. There is also evidence that kinesin localizes dynein to microtubule plus ends (Brendza et al., 2002; Zhang et al., 2003; Carvalho et al., 2004; Twelvetrees et al., 2016), suggesting that these motors could be directly coupled. Given these data, a central question is to determine how opposite-polarity motors are scaffolded.

[1]Department of Cellular and Molecular Medicine, University of California, San Diego, La Jolla, CA;   [2]Department of Cell Biology, Harvard Medical School, Boston, MA; [3]Department of Biochemistry and Molecular Genetics, University of Colorado Denver, Aurora, CO;   [4]Section of Cell and Developmental Biology, Division of Biological Sciences, University of California, San Diego, La Jolla, CA;   [5]Howard Hughes Medical Institute, Chevy Chase, MD.

*A.M. Dickey and W.B. Redwine contributed equally to this paper;   Correspondence to Samara L. Reck-Peterson: sreckpeterson@ucsd.edu;   W.B. Redwine's present address is Stowers Institute for Medical Research, Kansas City, MO;   P.T. Tran's present address is Department of Molecular and Cellular Biology, Harvard University, Cambridge, MA.   A preprint of this paper was posted in bioRxiv on December 31, 2018.

We and others have taken a "bottom-up" approach to study teams of motors by designing artificial scaffolds bearing opposite-polarity motors. For example, dynein and kinesin motors can be scaffolded by DNA origami (Derr et al., 2012) or short DNA oligomers (Belyy et al., 2016). Such approaches allow the basic biophysical properties of motor teams to be dissected. However, studies using physiological motor pairs and scaffolds are lacking, primarily because these scaffolds have not been identified or well characterized. One exception is our recent reconstitution of dynein transport to microtubule plus ends by a kinesin (Roberts et al., 2014), a process that occurs in vivo in yeast cells (Moore et al., 2009). In this system, cytoplasmic dynein-1 and the kinesin Kip2 required two additional proteins for scaffolding, and both motors were regulated so that Kip2-driven plus end–directed motility prevails (Roberts et al., 2014; DeSantis et al., 2017).

How are opposite-polarity motors scaffolded in mammalian cells? A group of proteins called "dynein activating adaptors" are emerging as candidate scaffolds (Reck-Peterson et al., 2018; Olenick and Holzbaur, 2019). Processive dynein motility requires an activating adaptor as well as the dynactin complex (McKenney et al., 2014; Schlager et al., 2014). Examples of activating adaptors include the Hook (Hook1, Hook2, and Hook3), BicD (BicD1, BicD2, BicDL1, and BicDL2), and ninein (Nin and Ninl) families of proteins (McKenney et al., 2014; Schlager et al., 2014; Redwine et al., 2017; Reck-Peterson et al., 2018; Olenick and Holzbaur, 2019). One piece of evidence supporting the role of activating adaptors as scaffolds is our recent identification of an interaction between Hook3 and the kinesin KIF1C using a proteomics approach (Redwine et al., 2017). KIF1C is a plus end–directed member of the kinesin-3 family (Dorner et al., 1998; Rogers et al., 2001), which has been implicated in the plus end–directed transport of secretory vesicles that move bidirectionally in multiple cell types (Schlager et al., 2010; Theisen et al., 2012). The dynein-activating adaptors BicD2 and BicDL1 may also interact with kinesin motors (Schlager et al., 2010; Splinter et al., 2010; Novarino et al., 2014). However, it is not known whether the interactions between dynein-activating adaptors and kinesins are direct, if dynein and kinesin binding is achieved simultaneously, or if the dynein activating adaptors can support motility in both directions.

Here we use Hook3 as a model system to determine if a physiological scaffold can link the opposite-polarity motors dynein and KIF1C to allow for motility in both the plus end and minus end directions. To do so, we perform complex in vitro reconstitutions with purified human dynein (1.4 MD and 12 subunits), dynactin (1.1 MD and 23 subunits), full-length Hook3 (166 kD as a dimer; see below), full-length KIF1C (246 kD as a dimer; see below), and microtubules. We identify the binding site for Hook3 on KIF1C and show that while Hook3 activates motility when added to dynein/dynactin, it does not activate motility when added to KIF1C. We also show that Hook3 scaffolds dynein/dynactin and KIF1C, resulting in motility toward either the microtubule plus or minus end without directional switching. In cells, we show that KIF1C recruits Hook3 to the cell periphery and that this requires the Hook3-binding site we identified. Together, this represents the first example of a fully

reconstituted physiological scaffold with opposite-polarity motors and identifies an excellent model system to continue to understand the complicated process of bidirectional motility seen in cells.

Results

Endogenous KIF1C and Hook3 interact specifically

We identified the Hook3–KIF1C interaction using a proximity-dependent biotinylation technique that relies on a promiscuous biotin ligase (BioID) with BioID-tagged Hook3 (Roux et al., 2012; Redwine et al., 2017). KIF1C is a kinesin-3 family member that is closely related to KIF1A and KIF1B (Dorner et al., 1998). It contains an amino-terminal motor domain and carboxy-terminal "tail" domain with several regions of predicted coiled-coil, a forkhead-associated domain, and a proline-rich region (Miki et al., 2005; Fig. 1 A). KIF1C interacts with the carboxy terminus of Hook3 (Redwine et al., 2017), while dynein and dynactin interact with Hook3's amino terminus (McKenney et al., 2014; Fig. 1 A).

Here, we began by performing a BioID experiment with BioID-tagged KIF1C to identify the protein interactome of KIF1C. To perform this experiment with near-endogenous expression levels of KIF1C (to avoid artifacts of protein overexpression), we generated KIF1C knockout 293T human cell lines using CRISPR/Cas9-based gene editing. Cotransfection of 293T cells with Cas9 and guides specific for exon 3 of the KIF1C genomic sequence or empty vector, followed by clonal selection, yielded two clones with full depletion of KIF1C and a control cell line (Fig. 1 B). We then infected one of these cell lines (KIF1C^{KO}, clone #1) and the control cell line with retroviral KIF1C-BioID-3xFLAG or BioID-3xFLAG plasmids driven by the murine stem cell virus (MSCV) promoter to generate stable cells expressing exogenous KIF1C-BioID or BioID alone (Behrends et al., 2010). The KIF1C protein expression levels in these cells were similar to endogenous KIF1C expression levels in 293T cells (Fig. 1 C). To perform BioID experiments, we lysed cells after growth in biotin-containing medium and isolated biotinylated proteins using streptavidin beads. Biotinylated proteins were identified by mass spectrometry (MS), and significant "hits" were determined using a label-free proteomics approach by comparison to a BioID-alone control (Zhang et al., 2010; Redwine et al., 2017). Proteins not present in the BioID control or with an enrichment ratio greater than threefold and a P value >0.05 relative to the control were considered significant hits. One of the top hits from this experiment was Hook3 (Fig. 1 D and Table S1). We did not detect other dynein-activating adaptors, except for Hook1, which was a significant hit, but had a relatively low peptide count.

To further characterize the interaction between KIF1C and Hook3, we immunoprecipitated endogenous KIF1C and Hook3 from 293T cells. Immunoblots with antibodies against Hook3 and KIF1C demonstrated that these proteins coprecipitate (Fig. 1 E). Because there are three different HOOK homologues in the human genome (HOOK1, HOOK2, and HOOK3) and because we detected both Hook3 and Hook1 in our KIF1C BioID data, we next used immunoprecipitation experiments to confirm these interactions and to determine if KIF1C interacted with the third Hook
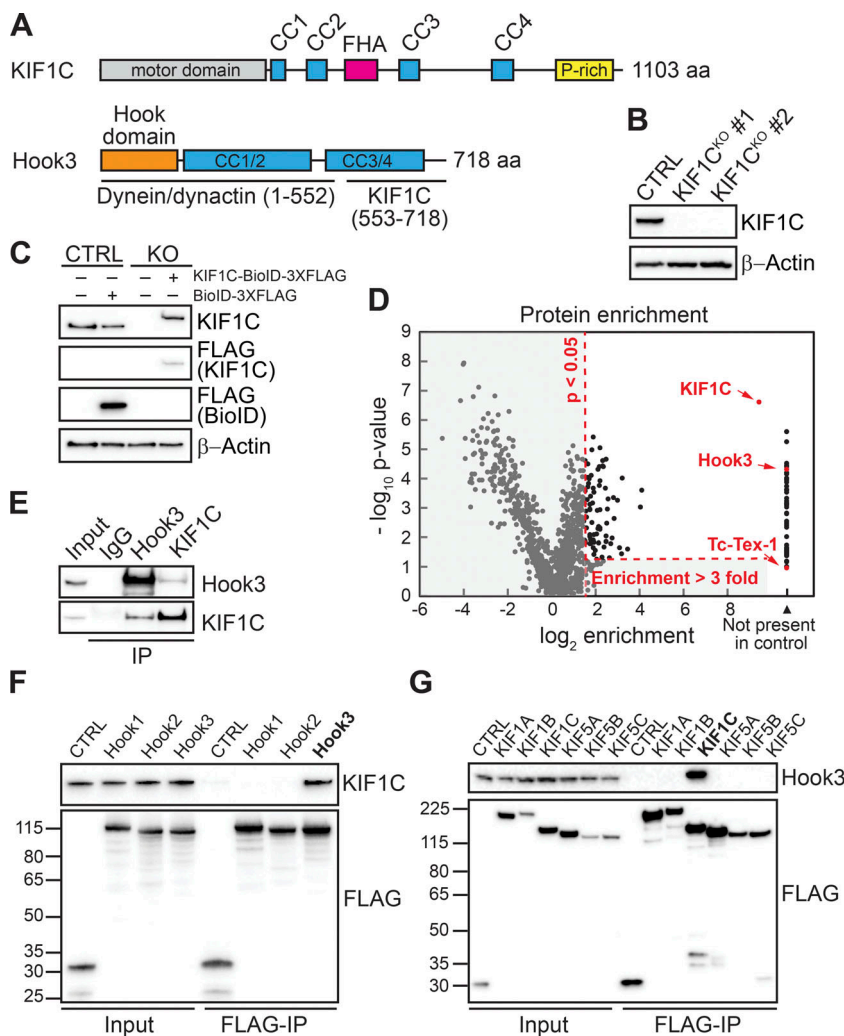
Kendrick et al.
Hook3 is a scaffold for opposite-polarity motors

Journal of Cell Biology
https://doi.org/10.1083/jcb.201812170

2983

Figure 1. **Endogenous Hook3 and KIF1C interact specifically. (A)** Domain organization of KIF1C and Hook3. KIF1C contains an amino-terminal kinesin motor domain and regions of predicted coiled coil (CC), a forkhead-associated domain (FHA), and a proline-rich (P-rich) region in its carboxy-terminal tail. Hook3 is largely made up of regions of predicted CC and contains dynein/dynactin and KIF1C-binding regions (McKenney et al., 2014; Redwine et al., 2017). The Hook domain, which is also involved in dynein binding (Schroeder and Vale, 2016), is indicated. **(B)** 293T cells were transfected with control CRISPR/Cas9 (CTRL) or with CRISPR/Cas9-gRNA specific for *KIF1C*. *KIF1C* knockout (KIF1C^{KO}) was confirmed in two different clones by immunoblotting with an anti-KIF1C antibody. Clone #1 was selected for further assays. β-Actin provided a loading control. **(C)** KIF1C^{KO} cells were infected with viral particles encoding MSCV-driven KIF1C-BioID-3xFLAG plasmid to obtain near-endogenous KIF1C-BioID protein expression levels. Immunoblots were performed using the indicated antibodies. β-Actin provided a loading control. **(D)** A volcano plot showing enrichment versus significance of proteins identified in KIF1C-BioID experiments relative to control (BioID alone) experiments. Proteins not present in the BioID control or with an enrichment ratio greater than threefold and a P value >0.05 relative to the control (dashed red lines) were considered significant hits. KIF1C, Hook3, and Tc-Tex-1 (DYNLT1, a dynein light chain) are marked in red. **(E)** Immunoprecipitation (IP) of endogenous Hook3 and KIF1C with the indicated antibodies from 293T cells. Immunoblots were performed with anti-Hook3 or KIF1C antibodies. **(F)** Human Hook1, Hook2, and Hook3 tagged with the HaloTag on their amino termini and 3xFLAG on their carboxy termini were transiently transfected into 293T cells and immunoprecipitated with FLAG affinity resin (FLAG-IP). Immunoblots were performed with anti-KIF1C and anti-FLAG antibodies. 3xFLAG-sfGFP provided a control. Protein molecular weight markers are shown in kilodaltons on the anti-FLAG immunoblot. **(G)** Human KIF1A, KIF1B, KIF1C, KIF5A, KIF5B, and KIF5C were each tagged with BioID-3xFLAG on their carboxy termini and stably expressed in 293T cells. Tagged proteins were immunoprecipitated with FLAG affinity resin (FLAG-IP), and immunoblots were performed with anti-Hook3 and anti-FLAG antibodies. BioID-3xFLAG provided a control. Protein molecular weight markers are shown in kilodaltons on the anti-FLAG immunoblot.

homologue, Hook2. We expressed each Hook homologue with an amino-terminal HaloTag and a carboxy-terminal 3xFLAG tag in 293T cells. Immunoprecipitation of each tagged Hook protein, followed by immunoblots for endogenous KIF1C, revealed that endogenous KIF1C coprecipitates with Hook3, but not Hook1 or Hook2 (Fig. 1 F). The presence of Hook1 in our KIF1C BioID dataset was likely due to heterodimerization of Hook1 with Hook3, rather than Hook1 interacting with KIF1C, as in our previous BioID experiments with Hook1 and Hook3, we detected Hook1 in Hook3 datasets and vice versa (Redwine et al., 2017). This is also consistent with a previous study that suggested possible heterodimerization between Hook family members (Xu et al., 2008).

We next asked if Hook3 specifically interacts with KIF1C. The two most closely related kinesin-3 family members to KIF1C are KIF1A and KIF1B (Dorner et al., 1998). In addition, the kinesin-1s, KIF5A, KIF5B, and KIF5C, are well-characterized cargo-transporting plus end–directed motors. We expressed each of these kinesins with a carboxy-terminal BioID-3xFLAG tag in 293T cells. Immunoprecipitation of each tagged kinesin,

followed by immunoblots for endogenous Hook3, revealed that endogenous Hook3 coprecipitates with KIF1C, but not KIF1A, KIF1B, KIF5A, KIF5B, or KIF5C (Fig. 1 G). We conclude that endogenous Hook3 and KIF1C interact in a specific manner.

KIF1C is a processive plus end–directed motor, whose motility is not activated by Hook3

To further explore the interaction between KIF1C and Hook3, we purified full-length KIF1C tagged with SNAP and 3xFLAG tags at its carboxy terminus, and full-length Hook3 tagged with a HaloTag at its amino terminus and a 3xFLAG tag at its carboxy terminus from 293T cells. Each protein migrated as a single band when analyzed by SDS-PAGE (Fig. S1 A). Using total internal reflection fluorescence (TIRF) microscopy with tetramethylrhodamine (TMR)-labeled KIF1C-SNAP-3xFLAG and Alexa Fluor 405–labeled microtubules, we visualized the motile properties of KIF1C on microtubules. Single full-length KIF1C molecules moved processively toward the microtubule plus end (Fig. 2 A; Fig. S1, B–D; and Video 1) with an average velocity of
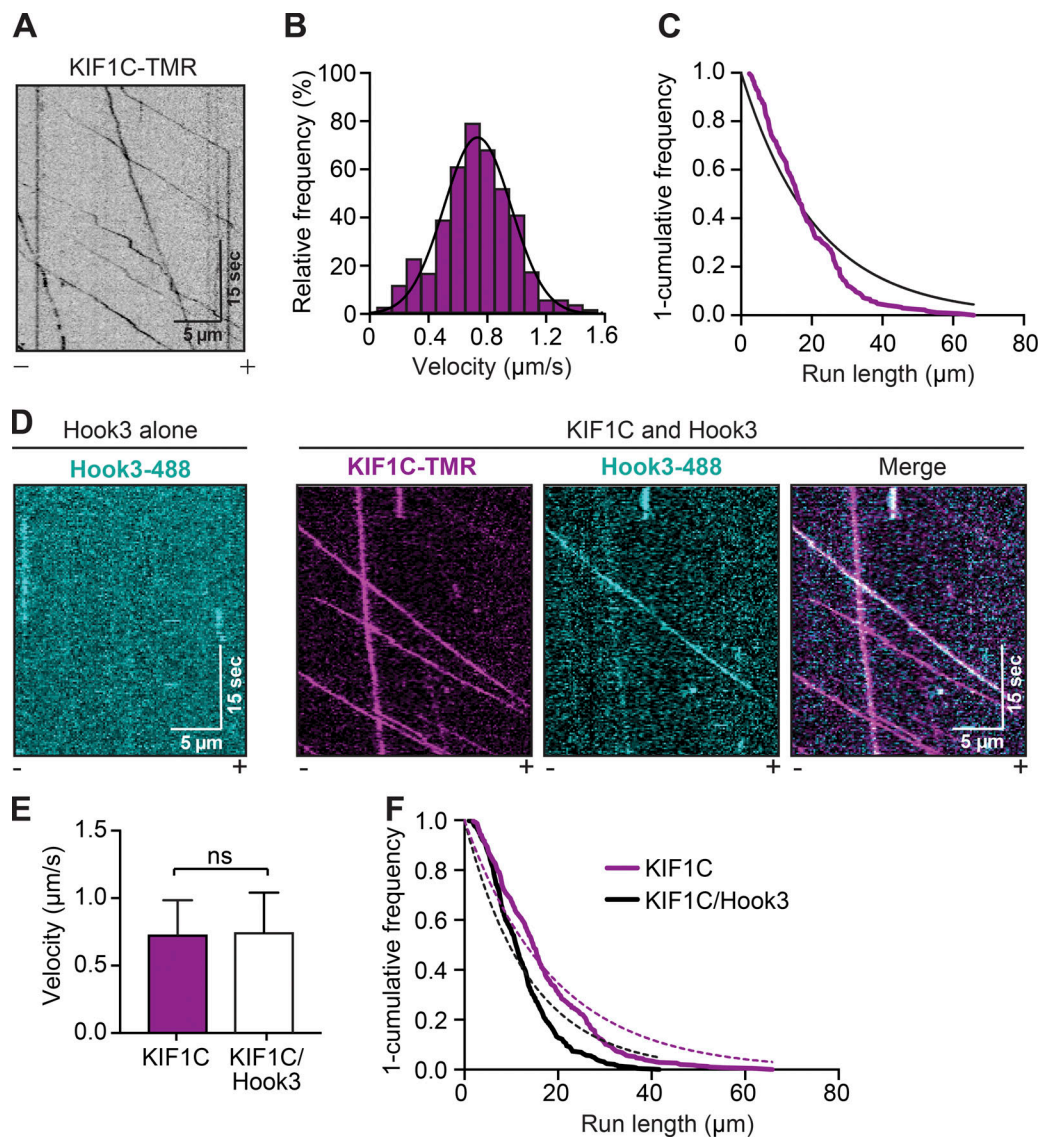
Kendrick et al.
Hook3 is a scaffold for opposite-polarity motors

Journal of Cell Biology 2984
https://doi.org/10.1083/jcb.201812170

Figure 2. **KIF1C is a highly processive kinesin-3 motor whose motility is not activated by Hook3. (A)** Representative kymograph from single-molecule motility assays with full-length KIF1C tagged with SNAP and 3xFLAG and labeled with TMR via the SNAP tag. Microtubule polarity is marked with minus (–) and plus (+). **(B)** A histogram of the velocity of single-KIF1C-TMR molecules fit to a Gaussian (black line, 0.734 ± 0.223 µm/s, mean ± SD, r^2 = 0.965). Data from three independent experiments are shown (n = 433). **(C)** Run length analysis of KIF1C-TMR. The 1-cumulative frequency distribution was fit to a one-phase exponential decay (black line). The representative mean decay constant is 21.11 µm (r^2 = 0.920, n = 158). **(D)** Representative kymographs from single-molecule motility assays with full-length Hook3 tagged at the amino terminus with an Alexa Fluor 488–labeled HaloTag and carboxy terminus with 3xFLAG (Hook3-488; left panel). KIF1C-TMR in the presence of Hook3-488 (right panels). Colocalized runs can be seen in the merge in white. Microtubule polarity is marked with minus (–) and plus (+). **(E)** Velocity (mean ± SD) of KIF1C-TMR–only runs compared with KIF1C-TMR runs in the presence of Hook3-488 (n = 433 for KIF1C only; n = 716 for KIF1C with Hook3). **(F)** Run length analysis from KIF1C-TMR–only runs compared with KIF1C-TMR runs in the presence of Hook3-488. The 1-cumulative frequency distribution was fit to a one-phase exponential decay (KIF1C, magenta dotted line; KIF1C with Hook3, black dotted line). The representative mean decay constant for KIF1C is 18.89 µm (r^2 = 0.932, n = 385) and for KIF1C with Hook3 is 13.77 µm (r^2 = 0.901, n = 418). Data were resampled with bootstrapping analysis, and statistical significance was calculated using an unpaired t test with Welch's correction; P = 0.0485. Representative data from three independent experiments are shown.

0.734 ± 0.223 µm/s (Fig. 2 B) and run length of 21.11 µm (Fig. 2 C). We next monitored the interaction of full-length KIF1C-TMR with full-length Hook3 (Fig. S1 A) labeled with Alexa Fluor 488 via its amino-terminal HaloTag using near-simultaneous two-color TIRF microscopy. Hook3 alone did not interact with microtubules (Fig. 2 D, left panel). In contrast, in the presence of KIF1C, Hook3 moved robustly toward microtubule plus ends and colocalized with KIF1C (Fig. 2 D, right panels; and Video 2). The presence of Hook3 did not alter KIF1C's dimerization state as indicated by photo-bleaching analysis (Fig. S1, C and E). KIF1C's velocity, landing rates, and pausing frequency were unchanged in the presence of Hook3, while a slight reduction in run length was observed (Fig. 2, E and F; and Fig. S1, C–G). In addition, the number of processive, diffusive, or static events for KIF1C was not significantly different in the presence or absence of Hook3 (Fig. S1 H). These data define the single-molecule motile
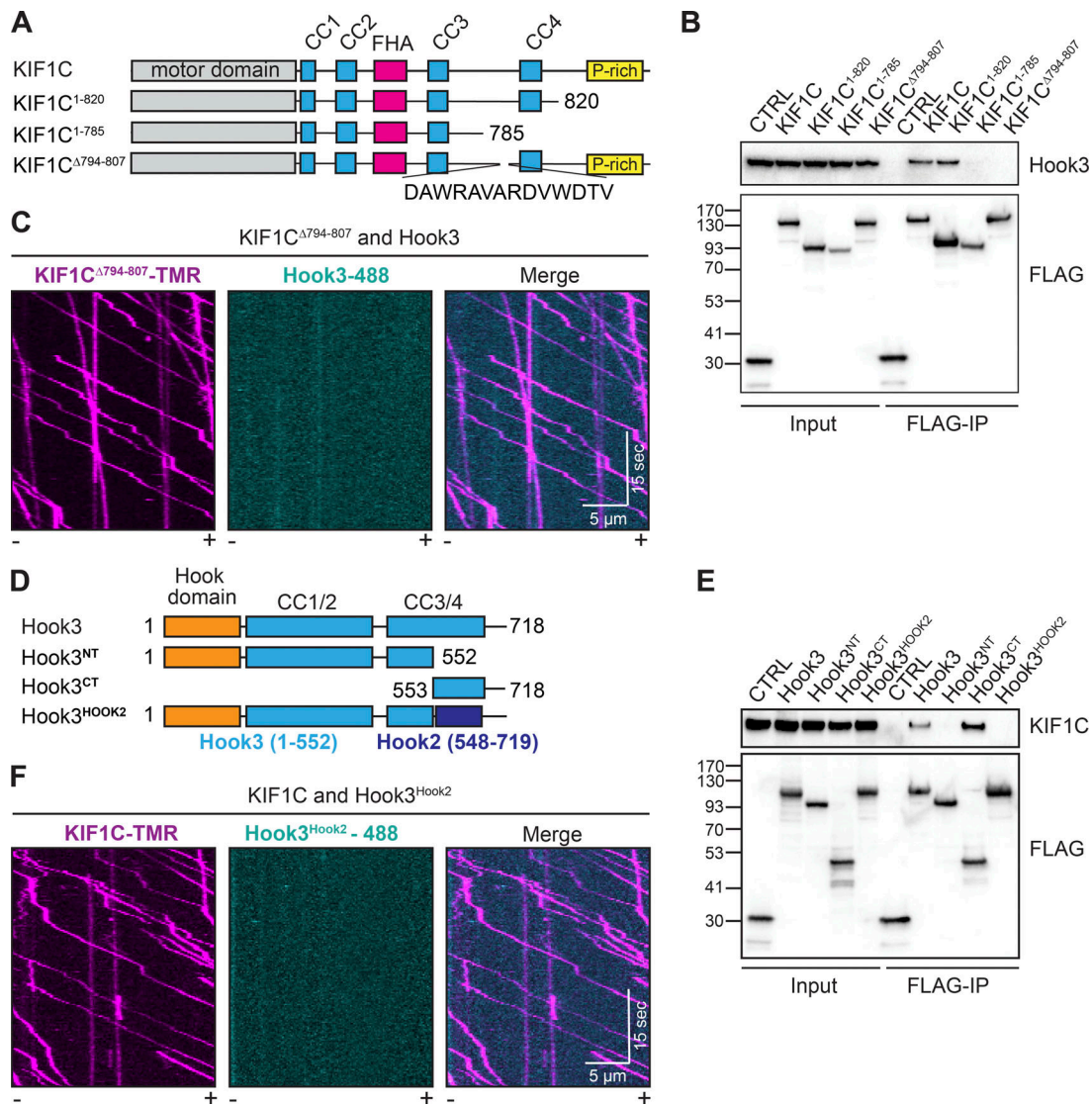
Figure 3. **14 amino acids in the tail of KIF1C mediate its interaction with Hook3. (A)** Schematic of constructs used to map the region of KIF1C that is responsible for binding to Hook3. **(B)** KIF1C-SNAP-3xFLAG constructs were transiently expressed in 293T cells and immunoprecipitated with FLAG affinity resin (FLAG-IP). Immunoblots were performed with anti-Hook3 and anti-FLAG antibodies. 3xFLAG-sfGFP provided a control. Protein molecular weight markers are shown in kilodaltons on the anti-FLAG immunoblot. **(C)** Representative kymographs from single-molecule motility assays with purified KIF1C$^{\Delta794-807}$-TMR in the presence of Hook3-488. Microtubule polarity is marked with minus (−) and plus (+). **(D)** Schematic of constructs used to map the region of Hook3 that is responsible for binding to KIF1C. Hook3^{NT} (aa 1–552), Hook3^{CT} (aa 553–718), Hook3^{Hook2} (a Hook3 [aa 1–552] and Hook2 [aa 548–719] chimera). **(E)** HaloTag-Hook3-3xFLAG constructs were transiently expressed in 293T cells and immunoprecipitated with FLAG affinity resin (FLAG-IP). Immunoblots were performed with anti-KIF1C and anti-FLAG antibodies. 3xFLAG-sfGFP provided a control. Protein molecular weight markers are shown in kilodaltons on the anti-FLAG immunoblot. **(F)** Representative kymographs from single-molecule motility assays of KIF1C-TMR in the presence of Hook3^{Hook2}-488. Microtubule polarity is marked with minus (−) and plus (+).

properties of KIF1C and show that Hook3 comigrates with processive KIF1C molecules and only minimally affects KIF1C's motile properties.

14 amino acids in the tail of KIF1C are required for Hook3 binding

We next sought to identify the regions in both KIF1C and Hook3 responsible for their interaction. We began with KIF1C, generating a series of carboxy-terminal KIF1C truncation constructs, all of which contained a carboxy-terminal 3xFLAG tag (Fig. 3 A). We made constructs lacking the carboxy terminus including the

proline-rich region (KIF1C$^{1-820}$) and lacking the fourth coiled-coil and the proline-rich region (KIF1C$^{1-785}$), and a deletion mutant that removed a short stretch of charged residues as well as two tryptophans (KIF1C$^{\Delta794-807}$-3xFLAG; Fig. 3 A). We hypothesized that the amino acid content in this region might form a protein–protein interaction interface in the KIF1C tail sequence that is otherwise predicted to be mainly unstructured or coiled-coil. Overexpression of these constructs in 293T cells followed by FLAG immunoprecipitations revealed that Hook3 binding to KIF1C is lost when the 14 aa (794–807) between coiled-coils 3 and 4 are deleted (Fig. 3 B). To confirm the requirement of this

region for the interaction between KIF1C and Hook3, we purified KIF1C$^{\Delta794-807}$ with carboxy-terminal SNAP tags and 3xFLAG tags from 293T cells (Fig. S2 A) and labeled it with TMR via its SNAP tag. Purified KIF1C$^{\Delta794-807}$ showed similar motile properties to wild-type KIF1C in a single-molecule assay (Fig. S2, B–D; and Video 3). However, when KIF1C$^{\Delta794-807}$-TMR was incubated with Hook3-488 and imaged using two-color TIRF microscopy, we observed no colocalized events, further demonstrating the importance of this region for Hook3 binding (Fig. 3 C and Video 4). We also made point mutations within this 14-aa region, but were unable to further refine the Hook3-binding site on KIF1C (Fig. S2 E). Taken together, our domain mapping identified a 14-aa region in the KIF1C tail that is necessary for Hook3 binding.

Next, we set out to map KIF1C's binding site on Hook3. We previously showed that the carboxy-terminal region of Hook3 (aa 553–718) is required for the KIF1C interaction (Redwine et al., 2017). To attempt to map this binding site more precisely, we generated a series of constructs lacking various regions in the carboxy-terminal tail of Hook3. However, these constructs failed to identify a single linear binding site (Fig. S2 F), perhaps because the KIF1C-binding site on Hook3 requires a folded domain. As an alternative approach to generate a Hook3 construct that could no longer bind KIF1C, we designed a chimeric construct in which we replaced aa 553–718 of the Halo-Hook3-3xFLAG construct with the homologous region of Hook2 (aa 548–719; Fig. 3 D and Fig. S2 G), which we showed could not bind KIF1C (Fig. 1 F). We then transfected this chimeric construct (Hook3^{Hook2}), full-length Hook3, Hook3 lacking the carboxy-terminal region (Hook3^{NT}), or Hook3 lacking the amino-terminal region (Hook3^{CT}) into 293T cells and performed FLAG immunoprecipitations. Only full-length Hook3 or Hook3^{CT} coimmunoprecipitated with endogenous KIF1C (Fig. 3 E). To verify that this chimeric Hook3^{Hook2} construct does not directly interact with KIF1C, we purified it from insect cells (Fig. S2 H) and labeled it with Alexa Fluor 488 via its HaloTag. Using two-color TIRF microscopy, we showed that the Hook3^{Hook2} chimera does not colocalize with KIF1C-TMR in a single-molecule motility assay (Fig. 3 F and Video 5).

Purified full-length Hook3 is a robust dynein-activating adaptor

Having shown that Hook3 and KIF1C directly interact, we next tested the dynein-activating ability of Hook3 in an in vitro system. Hook3 is a well-established dynein-activating adaptor (McKenney et al., 2014). However, in vitro studies are limited to analyses with a purified truncated version of Hook3 (aa 1–552, Hook3^{NT}) or full-length Hook3 present in cell lysates (Olenick et al., 2016), rather than purified full-length protein. In addition, since full-length BicD2, another dynein-activating adaptor, exists in an autoinhibited state (Stuurman et al., 1999; Hoogenraad et al., 2001), we aimed to characterize the dynein activation properties of purified full-length Hook3 and establish if full-length Hook3 is autoinhibited.

To do so, we purified human dynein and dynactin complexes separately from stable 293T cell lines expressing the dynein intermediate chain (IC2) or the dynactin subunit p62 tagged with the SNAP tag or HaloTag, respectively, and a 3xFLAG tag (Redwine et al., 2017). We labeled IC2 with Alexa Fluor 647 and

used nonfluorescently labeled dynactin for these experiments. In the absence of Hook3, the dynein/dynactin complex is largely stationary in single-molecule motility assays, exhibiting occasional diffusive events and very rare motile events (Fig. S3 A). In the absence of dynein, Hook3 and dynactin are not motile (Fig. S3 B). However, the combination of dynein, dynactin, and purified full-length Hook3 led to robust activation of dynein motility toward microtubule minus ends (Fig. 4 A and Video 6). The velocity (0.658 ± 0.287 µm/s; Fig. 4 B) and run length (21.65 µm; Fig. 4 C) were comparable to the values we obtained with truncated Hook3^{NT} (Fig. 4, D–F) and were also consistent with previously reported values for truncated Hook3 (McKenney et al., 2014; Schroeder and Vale, 2016; Redwine et al., 2017) or Hook3 present in cell lysates (Olenick et al., 2016). In addition, the chimeric Hook3^{Hook2} construct that does not bind KIF1C (Fig. 3, E and F) activated dynein/dynactin to a similar extent as full-length Hook3 (Fig. 4, G–I). Our analysis also showed that dynein/dynactin activated by Hook3 displayed no difference in pausing frequency or the number of processive, diffusive, or static events (Fig. S3, D and E). This suggests that purified full-length Hook3 is a robust dynein activator and is not autoinhibited in its native state.

Hook3 is a scaffold for dynein/dynactin and KIF1C

Thus far, our experiments indicate that full-length Hook3 directly associates with KIF1C and binds to and activates dynein/dynactin complexes. We next sought to determine if Hook3 could bind KIF1C and the dynein/dynactin complex simultaneously. To test this, we performed three-color TIRF microscopy experiments with purified proteins. For these experiments, IC2 was labeled with Alexa Fluor 647, Hook3 with Alexa Fluor 488, and KIF1C with TMR, and dynactin was unlabeled. This experimental setup allowed us to detect moving events corresponding to (1) KIF1C alone, (2) KIF1C with Hook3, (3) dynein/dynactin with Hook3, and (4) KIF1C with dynein/dynactin and Hook3 (Fig. 5 A). The presence of dynactin is inferred because it is required for dynein motility (McKenney et al., 2014; Schlager et al., 2014). Complexes that contained all three labeled components (dynein-647, Hook3-488, and KIF1C-TMR) moved in either the minus end (Fig. 5 B, top panel) or plus end (Fig. 5 B, bottom panel) directions (Videos 7 and 8). The presence of these three-color colocalized events implies that Hook3 scaffolds dynein/dynactin and KIF1C to form a complex capable of moving toward the microtubule plus end or minus end. We did not observe three-color colocalized runs when Hook3 was omitted from the mixture (Fig. S4 A) or when TMR-labeled KIF1C$^{\Delta794-807}$ (Fig. S4 B) or Alexa Fluor 488–labeled Hook3^{Hook2} (Fig. S4 C) was used as opposed to their full-length wild-type counterparts.

Next, we quantified the velocity and run length of each detectable species (Fig. 5 C and Fig. S4, D and E). Complexes containing KIF1C and dynein/dynactin scaffolded by Hook3 had slower velocities in the minus end direction compared with complexes lacking KIF1C (Fig. 5 C). The slowing of the scaffolded complexes in the minus end direction suggests that KIF1C may engage the microtubule when dynein is the primary driver of motility. Notably, we did not observe any runs (71 of 856 runs
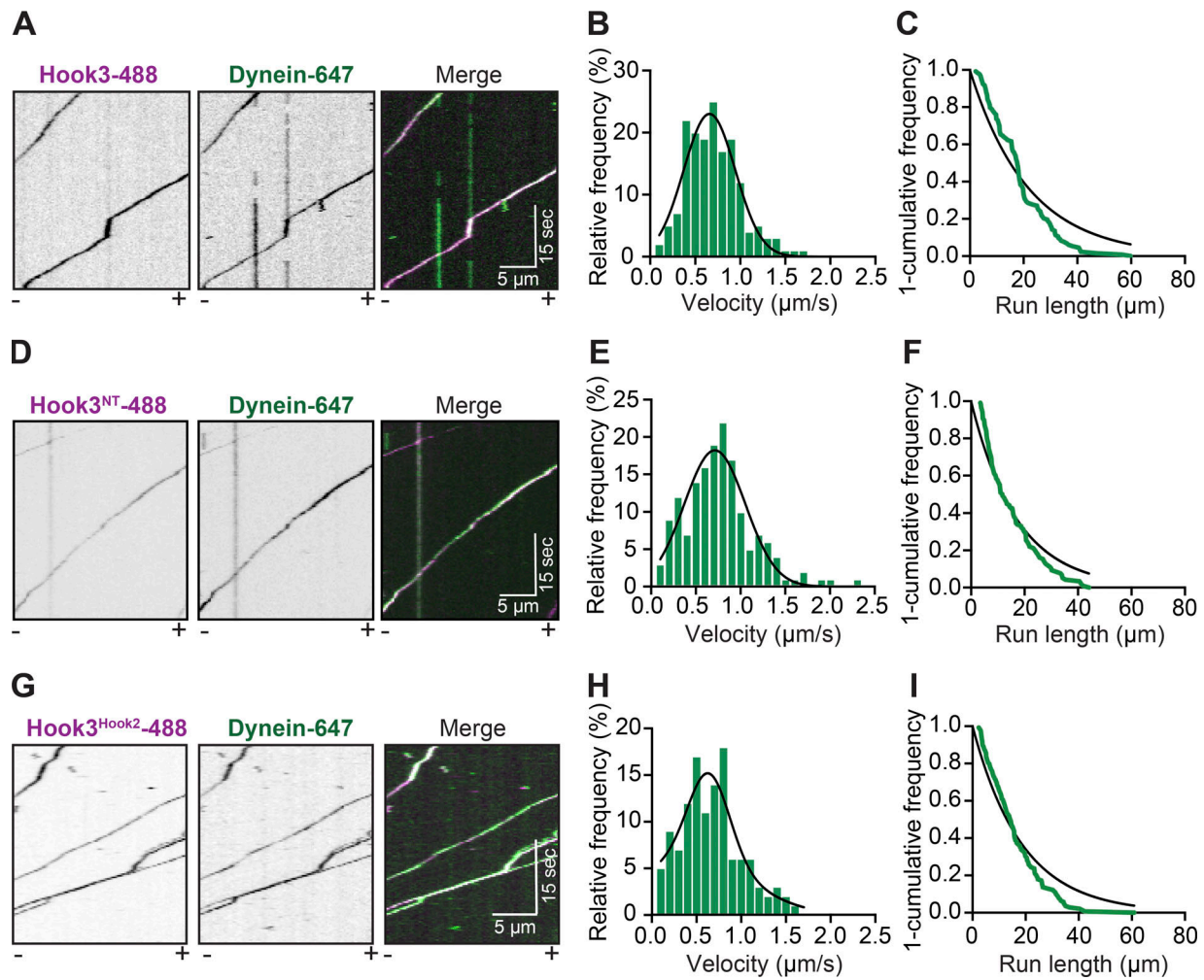
Kendrick et al.
Hook3 is a scaffold for opposite-polarity motors

Journal of Cell Biology
https://doi.org/10.1083/jcb.201812170

2987

Figure 4. **Purified full-length Hook3 activates dynein motility. (A)** Representative kymographs from single-molecule motility assays with purified dynein-647 (green), unlabeled dynactin, and full-length Hook3-488 (magenta). Microtubule polarity is marked with minus (–) and plus (+). **(B)** A histogram of dynein/dynactin velocity in the presence of purified full-length Hook3 fit to a Gaussian (black line, 0.658 ± 0.287 μm/s, mean ± SD, r^2 = 0.910). Representative data from three independent experiments are shown (n = 166). **(C)** Run length analysis of dynein/dynactin in the presence of full-length Hook3. The 1-cumulative frequency distribution (green line) was fit to a one-phase exponential decay (black line). The representative mean decay constant is 21.65 μm (r^2 = 0.902, n = 133). **(D)** Representative kymographs from single-molecule motility assays with purified dynein-647 (green), unlabeled dynactin, and Hook3$^{1-552}$-488 (magenta). Microtubule polarity is marked with minus (–) and plus (+). **(E)** A histogram of dynein/dynactin velocity in the presence of Hook3$^{1-552}$ fit to a Gaussian (black line, 0.710 ± 0.340 μm/s, mean ± SD, r^2 = 0.931). Representative data from two independent experiments are shown (n = 158). **(F)** Run length analysis of dynein/dynactin in the presence of Hook3$^{1-552}$. The 1-cumulative frequency distribution (green line) was fit to a one-phase exponential decay (black line). The representative mean decay constant is 17.08 μm (r^2 = 0.938, n = 118). **(G)** Representative kymographs from single-molecule motility assays with purified dynein-647 (green), unlabeled dynactin, and the Hook3^{Hook2}-488 chimera (magenta). Microtubule polarity is marked with minus (–) and plus (+). **(H)** A histogram of velocity of dynein/dynactin in the presence of the Hook3^{Hook2} chimera fit to a Gaussian (black line, 0.606 ± 0.345 μm/s, mean ± SD, r^2 = 0.813). Representative data from three independent experiments are shown (n = 122). **(I)** Run length analysis of dynein/dynactin in the presence of the Hook3^{Hook2}-488 chimera. The 1-cumulative frequency distribution (green line) was fit to a one-phase exponential decay (black line). The representative mean decay constant is 21.25 μm (r^2 = 0.934, n = 139).

contained both motors) in which the moving molecules changed direction.

Because we observed more minus end– versus plus end–directed runs when both KIF1C and dynein were present in the moving complexes (Fig. 5 D), we wondered if the number of runs in either direction was dictated by the amount of each motor available for Hook3 binding. To test this, we varied that relative ratio of KIF1C to dynein in our experiments. These experiments were performed with labeled dynein (Alexa Fluor 647) and Hook3 (Alexa Fluor 488), and unlabeled dynactin and KIF1C. We

did not label KIF1C so that we could increase its concentration and still observe single-molecule events. Due to the lack of a label on KIF1C, we could detect three separate moving events: (1) plus end–directed runs that were only Hook3/KIF1C, (2) plus end–directed runs that contained both dynein and KIF1C, and (3) minus end–directed runs that contained two species, dynein/dynactin/Hook3 and dynein/dynactin/Hook3 with KIF1C. As the KIF1C concentration was increased relative to dynein, we observed an increase in the percentage of plus end–directed runs containing both dynein and KIF1C, as well as the number of
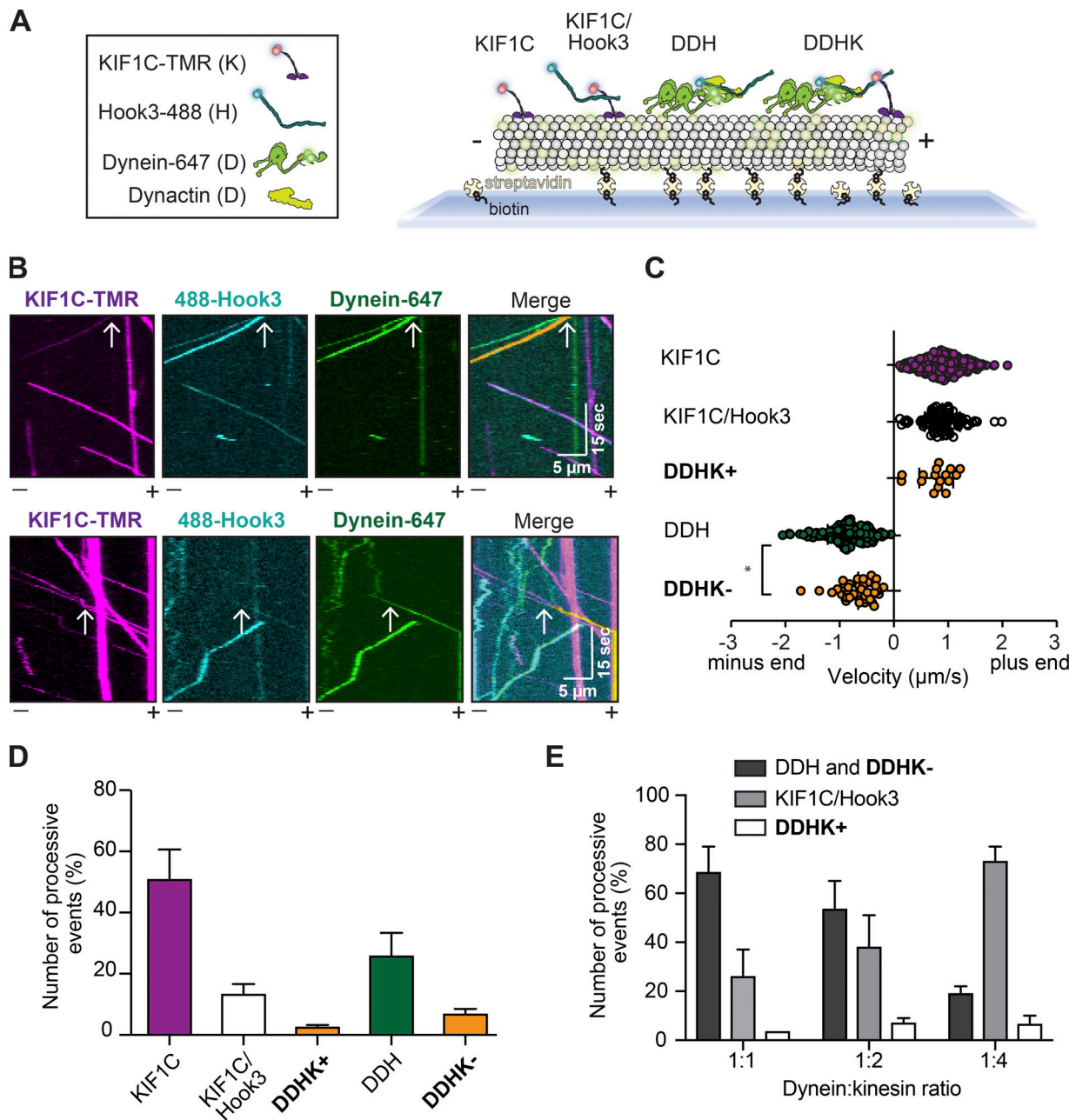
Figure 5. **Hook3 is a scaffold for opposite-polarity motors. (A)** Schematic of the experimental set up for three-color single-molecule motility assays. Four different species are detectable using three-color imaging: (1) KIF1C-TMR (KIF1C), (2) KIF1C-TMR with Hook3-488 (KIF1C/Hook3), (3) dynein-647 with dynactin and Hook3-488 (DDH), and (4) dynein-647 with dynactin, Hook3-488, and KIF1C-TMR (DDHK). **(B)** Representative kymographs from single-molecule motility assays with purified dynein-647, unlabeled dynactin, KIF1C-TMR, and Hook3-488. A three-color colocalized minus end–directed run (top panel) and three-color colocalized plus end–directed run (bottom panel) are marked with white arrows on each single-channel image and in the merge. The yellow signal in the merge highlights the colocalized run. Microtubule polarity is marked with minus (–) and plus (+). **(C)** Velocity analysis of the indicated complexes (KIF1C, n = 345; KIF1C/Hook3, n = 136; DDHK+, n = 18; DDH, n = 304; DDHK−, n = 53). Statistical significance was calculated with a one-way ANOVA with Tukey post-test; *, P = 0.0121. Combined data from four independent experiments is shown. **(D)** Percent processive events (mean ± SEM) reported in C. Combined data from four independent experiments is shown. **(E)** Percent processive events (mean ± SEM) in the two-color assay with purified dynein-647, unlabeled dynactin, Hook3-488, and unlabeled KIF1C. Increasing concentrations of unlabeled KIF1C are used as indicated by the dynein:KIF1C ratio. Combined data from three independent experiments is shown.

Hook3/KIF1C runs. We also observed a corresponding decrease in the percentage of minus end–directed runs (Fig. 5 E). Overall these results imply that the binding of dynein and KIF1C to Hook3 could be competitive. Velocity and run length analyses of these events were comparable to the values we obtained in the three-color experiments (Fig. 5 C and Fig. S4, D–I). These data suggest that Hook3 might have different affinities for each motor. In cells, this could result in differences in complex formation or directionality depending on local cellular concentrations of each motor.

KIF1C recruits Hook3 to the cell periphery

Thus far, our data indicate that Hook3 and KIF1C directly interact and that Hook3 can scaffold complexes containing both dynein/dynactin and kinesin. We next explored whether these interactions take place in a cellular context. To test this, we took advantage of our KIF1C 293T knockout cells (Fig. 1 B). We infected KIF1C[KO] cells (clone #1) with MSCV-driven retroviral KIF1C-tagRFP or KIF1C[Δ794–807]-tagRFP plasmids to generate stable cells expressing exogenous KIF1C-tagged proteins and used confocal immunofluorescence microscopy to image the cells. Although the KIF1C-tagRFP or KIF1C[Δ794–807]-tagRFP protein expression levels in these cells were higher than in control 293T cells, this approach allowed us to account for the complete pool of KIF1C in the cell (Fig. 6 A). KIF1C knockout in these cells did not alter Hook3's localization (Fig. S5 A). However, full-length wild-type KIF1C recruited endogenous Hook3 to the cell periphery, and this recruitment was abolished in cells expressing KIF1C lacking the Hook3 binding region (Fig. 6, B and C). We also tested if dynactin was recruited to the cell periphery in a KIF1C-dependent manner, but did not observe relocalization of dynactin (Fig. S5, B and C).

Next, we asked if the KIF1C-binding region on Hook3 was required for KIF1C-dependent recruitment of Hook3 to the cell periphery. To do this, we cotransfected human U2OS cells with Hook3 (tagged with super folder GFP [sfGFP]) and KIF1C (tagged with V5) plasmids and visualized their localization using confocal immunofluorescence microscopy. sfGFP alone or sfGFP tagged Hook3 constructs, including full-length Hook3, Hook3[NT], and Hook3[CT], where expressed in U2OS cells in the presence or absence of KIF1C. Expression of these constructs alone in U2OS cells led to mainly cytoplasmic Hook3 localization, similar to endogenous Hook3 distribution in these cells (Fig. S5, D and E). However, when KIF1C was coexpressed with Hook3 or Hook3[CT], Hook3 was enriched in KIF1C-V5 foci found at the cell periphery (Fig. 6, D and E). This enrichment was lost when Hook3[NT], which lacks the KIF1C-binding region, was coexpressed with KIF1C-V5 (Fig. 6, D and E). Together our data show that KIF1C recruits Hook3 to the cell periphery and that this recruitment depends on the binding sites we identified in both KIF1C and Hook3.

Discussion

Here we have shown that the dynein-activating adaptor Hook3 directly scaffolds the opposite-polarity motors cytoplasmic dynein-1/dynactin and the kinesin KIF1C. In doing so, we have reported the single-molecule motile properties of KIF1C in the presence and absence of full-length Hook3. We mapped the Hook3 interacting region on KIF1C to 14 aa in its tail. Hook3 and KIF1C also interact in a cellular environment, as KIF1C recruits Hook3 to the cell periphery. Full-length Hook3 does not activate the motile properties of KIF1C, but is required to activate dynein/dynactin motility. Finally, we reconstituted the entire dynein/dynactin/Hook3 and KIF1C complex from pure components and characterized its motile properties. While complexes containing both motors are relatively rare, we show that dynein/dynactin can transport KIF1C and KIF1C can transport dynein.

KIF1C is a highly processive motor whose activity is not activated by Hook3

Under our analysis conditions, full-length KIF1C is a highly processive motor with a characteristic run length that is >15 µm. Kinesin-1s are regulated by autoinhibition via interactions between their motor and tail domains (Friedman and Vale, 1999; Stock et al., 1999; Hackney and Stock, 2000). Several lines of evidence suggest that dimeric kinesin-3 family members are also autoinhibited (Yamada et al., 2007; Hammond et al., 2009; Farkhondeh et al., 2015). The fact that our purified full-length KIF1C alone is a robust processive motor may indicate that it is not autoinhibited. It is also possible that KIF1C as purified from human 293T cells contains posttranslational modifications that could relieve autoinhibition. High-throughput proteomics approaches suggest that KIF1C is phosphorylated, as well as monomethylated, in multiple regions in its tail (Hornbeck et al., 2015). However, how phosphorylation or other candidate posttranslational modifications affect KIF1C's motor activity has not been investigated. In our experiments, the addition of Hook3 had no effect on KIF1C's velocity, pausing frequency, or landing frequency, and caused a modest decrease in KIF1C's run length. This suggests that Hook3 is not required to activate KIF1C motility, but rather that Hook3 may function to link KIF1C to other proteins or cargos. In addition, our data suggest that KIF1C exists as a dimer in the presence or absence of Hook3. It is likely that KIF1C interacts with a Hook3 homodimer based on previous evidence showing that Hook proteins, as well as other dynein-activating adaptors, form dimers alone or when in a complex with dynein/dynactin (Urnavicius et al., 2015; Schroeder and Vale, 2016; Lee et al., 2018).

Simultaneous with our work, another group reported the motile properties of KIF1C (Siddiqui et al., 2019). In that study, KIF1C purified from insect cells appeared to be largely inactive as observed by single-molecule motility experiments. The addition of Hook3 or deletion of a region of KIF1C's third predicted coiled-coil domain increased the landing rate of KIF1C. In contrast, we did not observe a difference in landing rate in the presence of Hook3. The differences between our results and that work (Siddiqui et al., 2019) could be due to the source of the protein, posttranslational state of the protein, purification methods, or motility assay conditions. Further work will be required to differentiate among these possibilities.

Hook3 is a scaffold for bidirectional motility

Our three-color single-molecule experiments show that Hook3, KIF1C, and dynein/dynactin can exist in a complex together. Furthermore, complex formation requires the KIF1C binding site we identified, and the complex does not form when the carboxy terminus of Hook3 is replaced by the carboxy terminus of Hook2 (the Hook family member we showed did not bind KIF1C). Our analysis of fully reconstituted dynein/dynactin/Hook3 and KIF1C complexes indicates that KIF1C can transport dynein/dynactin toward microtubule plus ends and that dynein/dynactin can transport KIF1C toward microtubule minus ends. This suggests that opposite-polarity motor binding to Hook3 is not mutually exclusive. Simultaneous Hook3 binding to both motors negatively affects dynein's motility. At the concentrations used
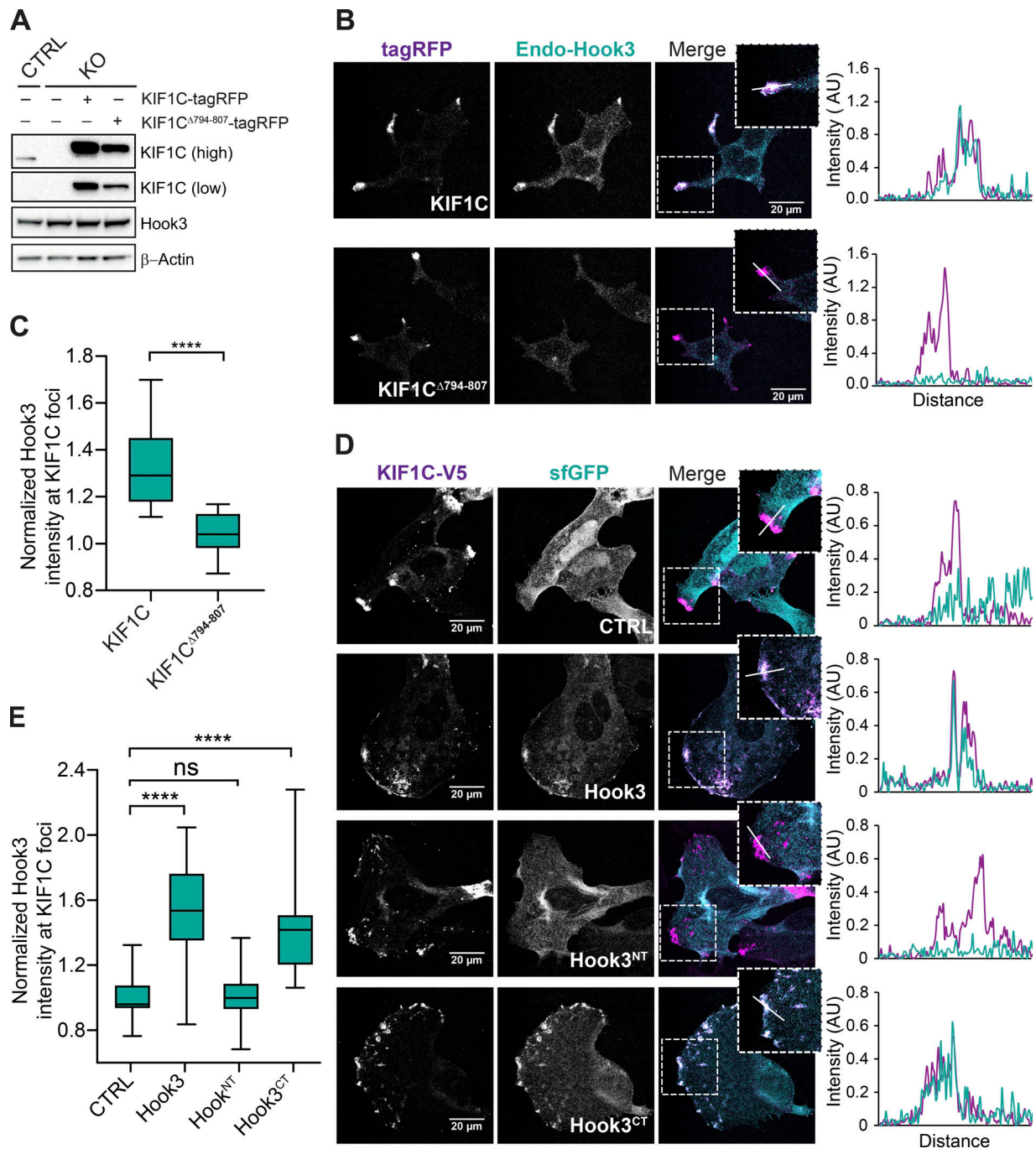
Kendrick et al.
Hook3 is a scaffold for opposite-polarity motors

Journal of Cell Biology 2990
https://doi.org/10.1083/jcb.201812170

Figure 6. **KIF1C recruits Hook3 to the cell periphery. (A)** 293T KIF1C[KO] cells (KO) were infected with viral particles encoding MSCV-driven KIF1C-tagRFP-3xFLAG or KIF1C[Δ794-807]-tagRFP-3xFLAG plasmids. Immunoblots were performed with the indicated antibodies. Low and high exposures with the KIF1C antibody are shown. β-Actin provided a loading control. 293T cells transfected with CRISPR-Cas9 (CTRL) were used as control cells. **(B)** Confocal microscopy of KIF1C and Hook3 localization in stable 293T cell lines expressing KIF1C-tagRFP-3xFLAG or KIF1C[Δ794-807]-tagRFP-3xFLAG. Cells were grown on glass coverslips, fixed, and stained for endogenous Hook3 (Endo-Hook3). The tagRFP and Hook3 signals are shown in representative maximum intensity projections. The overlap of intensity profiles (AU) generated from drawing a 15-µm line segment across individual z-sections is shown to the right of the images. **(C)** The mean normalized Hook3 intensity within KIF1C foci for KIF1C-tagRFP-3xFLAG (n = 25) or KIF1C[Δ794-807]-tagRFP-3xFLAG (n = 24). Foci were determined by thresholding the KIF1C image, and masks of these foci were used to measure the Hook3 intensity in the corresponding regions in maximum projection images. Box plots represent the maximum and minimum values. Statistical significance was calculated with an unpaired t test. ****, $P < 0.0001$. Representative data from three independent experiments is shown. **(D)** Confocal microscopy of KIF1C and Hook3 in U2OS cells. Cells were grown on glass coverslips and transiently cotransfected with the indicated sfGFP-tagged Hook3 (full-length Hook3, Hook3[NT] [aa 1–552], and Hook3[CT] [aa 553–718]) or control sfGFP constructs, and KIF1C-V5. 24 h after transfections, cells were fixed and stained with V5-specific antibody. The V5 and sfGFP signals are shown in representative maximum intensity projections. The overlap of intensity profiles (AU) generated from drawing a 15-µm line segment across an individual z-section is shown to the right of the images. **(E)** The mean normalized Hook3 intensity within KIF1C foci for cells transfected with different Hook3 constructs (CTRL, n = 27; Hook3, n = 28; Hook3[NT], n = 33; Hook3[CT], n = 29). Foci were determined by thresholding the KIF1C image, and masks of these foci were used to measure the Hook3 intensity in these corresponding regions in maximum projection images. Box plots represent maximum and minimum values. Statistical significance was calculated with one-way ANOVA with Tukey post-test, ****, $P < 0.0001$. Representative data from three independent experiments is shown. ns, not significant.

in our assays, it appears that a higher fraction of Hook3 associates with dynein than with KIF1C, which could indicate that Hook3 has a higher affinity for dynein than for KIF1C. Our analysis raises the possibility that dynein and KIF1C may compete for Hook3 binding. We also note that complexes containing both motors are relatively rare, suggesting that interaction of Hook3 with each motor could be regulated in cells. A detailed analysis of various binding affinities and complex stoichiometry will require higher purification yields of all components.

We do not observe any switches in direction, but we do observe that the presence of KIF1C can slow the velocity of dynein/dynactin/Hook3 complexes in the minus end direction. This is consistent with a model in which KIF1C engages microtubules while being pulled by dynein toward microtubule minus ends, thus slowing dynein's velocity. Similar velocity decreases have been observed with other opposite-polarity motor teams (Derr et al., 2012; Roberts et al., 2014; Belyy et al., 2016). Our data suggest that if dynein and KIF1C share a common cargo that moves bidirectionally, the activity of each motor type may be regulated to achieve changes in direction. If such factors exist, our reconstituted system is likely missing them as indicated by the lack of directional switching of dynein/dynactin/Hook3/KIF1C complexes and the purity of our components.

What is the physiological function of kinesin and dynein/dynactin complexes scaffolded by Hook3?

Our data do not directly determine the physiological role of dynein/dynactin complexes scaffolded to KIF1C by Hook3; however, our experiments and others in the literature suggest several possibilities, all of which will be exciting areas for future research.

First, it is possible that Hook3 scaffolds KIF1C and cytoplasmic dynein for the bidirectional motility of a shared cargos. Consistent with this, KIF1C cargos move bidirectionally in human epithelial cells and neurons (Schlager et al., 2010; Theisen et al., 2012). Multiple cargos for KIF1C have been proposed. KIF1C is implicated in the transport of α5β1-integrins for focal adhesion and podosome formation (Kopp et al., 2006; Theisen et al., 2012; Efimova et al., 2014). KIF1C has also been shown to bind to Rab6 (Lee et al., 2015), and KIF1C depletion leads to defects in synaptic vesicle transport (Schlager et al., 2014; Lipka et al., 2016). In contrast, the most likely cargos for Hook3 are endo-lysosomal compartments (Guo et al., 2016). Hook3 is part of the FHF complex, named after its components, Fused-Toes homologue (FTS), Hook-related protein, and FTS and Hook-interacting protein (FHIP; Xu et al., 2008; Bielska et al., 2014; Yao et al., 2014). FHF is thought to link the dynein/dynactin complex to Rab5-marked early endosomes, which move bidirectionally in both neurons and filamentous fungi (Bielska et al., 2014; Yao et al., 2014; Zhang et al., 2014; Guo et al., 2016).

Second, the functional role of Hook3 in scaffolding dynein and KIF1C could be to recycle one or both motors. Such recycling of dynein by kinesin has been observed in *Saccharomyces cerevisiae*, where dynein is transported to microtubule plus ends by a kinesin and a set of accessory proteins (Moore et al., 2009). This process is through direct protein–protein interactions, as it

has been reconstituted in vitro (Roberts et al., 2014). In addition, in *Drosophila melanogaster* oocytes, filamentous fungi, and neurons, kinesin-1 family members are required for dynein's plus end localization (Brendza et al., 2002; Zhang et al., 2003; Twelvetrees et al., 2016). If and how kinesins are recycled are less clear; one study of mammalian kinesin-1 suggests that diffusion is sufficient for its recycling (Blasius et al., 2013).

Finally, a third possible function of this complex could be to sequester Hook3 from the available pool of dynein/dynactin activating adaptors. Our cellular analysis shows that KIF1C recruits Hook3 to the cell periphery in a manner that depends on the binding sites we identified in both KIF1C and Hook3. By removing Hook3 from the cellular pool of dynein activators, KIF1C could be acting as a negative regulator of dynein/dynactin/Hook3 cargo motility. Our observation that KIF1C does not recruit dynactin to the cell periphery supports this possibility, at least in 293T cells.

Is scaffolding of dynein/dynactin and kinesin by dynein-activating adaptors a general principle?

We have directly demonstrated that the dynein-activating adaptor Hook3 scaffolds KIF1C and dynein/dynactin and that these complexes can move toward either the plus end or the minus end of microtubules. Do other dynein-activating adaptors perform similar functions for dynein/dynactin and other kinesins? There are hints in the literature that this may be the case. For example, interactions between KIF1C and both BicD2 and BicDL1 have also been suggested. In the case of BicD2, network analysis of genes mutated in hereditary spastic paraplegias, a disease associated with KIF1C mutations (Dor et al., 2014), identified BicD2 as a possible KIF1C interactor (Novarino et al., 2014). This interaction was confirmed by coimmunoprecipitation with overexpressed proteins (Novarino et al., 2014). In the case of BicDL1, it was shown to interact with KIF1C via two-hybrid experiments and endogenous KIF1C coimmunoprecipitated with overexpressed BicDL1 (Schlager et al., 2010). Other proteins that share a similar general domain structure to the bona fide dynein activating adaptors, such as TRAK1, TRAK2, and HAP1, are candidate dynein-activating adaptors (Reck-Peterson et al., 2018). Interestingly, TRAK1, TRAK2, and HAP1 have all been shown to interact with kinesin-1 family members and dynein/dynactin subunits (Engelender et al., 1997; Li et al., 1998; Twelvetrees et al., 2010; van Spronsen et al., 2013). Cell biological and in vitro reconstitution experiments will be required to determine if these candidate dynein-activating adaptors and other known dynein-activating adaptors scaffold dynein/dynactin to kinesin family members for bidirectional motility.

Materials and methods

Molecular cloning

All plasmids used in this study, unless otherwise stated, were constructed by PCR and Gibson isothermal assembly. BioID G2 (Kim et al., 2014) was a gift of K. Roux (Sanford School of Medicine, University of South Dakota, Vermillion, SD). P62 (isoform 1, 460 aa) was amplified from a human RPE1 cell cDNA

Kendrick et al.
Hook3 is a scaffold for opposite-polarity motors

Journal of Cell Biology 2992
https://doi.org/10.1083/jcb.201812170

library (generated in the Reck-Peterson laboratory). Hook3 (clone ID: 5106726), KIF1A (clone ID: 40037561), KIF1B (clone ID: 319918), KIF5A (clone ID: 40148192), KIF5B (clone ID: 8991995), and KIF5C (clone ID: 516562) cDNAs were obtained from Dharmacon. Hook1 (clone ID: HsCD00044030), Hook2 isoform 2 (clone ID: HsCD00326811), and KIF1C (clone ID: HsCD00336693) cDNAs were obtained from PlasmidID (Harvard Medical School, Boston, MA). Hook2 isoform 2 clone was mutagenized in the Reck-Peterson laboratory to generate Hook2 isoform 1. The Hook3[Hook2] chimera construct was generated by replacing Hook3 aa 553–718 with Hook2 aa 548–719 using Gibson isothermal assembly and cloned into pLIB vector containing an amino-terminal His_6-ZZ-TEV-HaloTag for expression in Sf9 cells. The pSpCas9(BB)-2A-Puro (PX459) V2.0 vector was a gift from F. Zhang (Broad Institute, Cambridge, MA; plasmid 62988; Addgene).

Cell lines and transfections
Human 293T and U2OS cells were obtained from ATCC and maintained at 37°C with 5% CO_2 in DMEM (Corning) supplemented with 10% FBS (Gibco) and 1% penicillin streptomycin (PenStrep; Corning). Sf9 cells were obtained from Thermo Fisher Scientific and grown in Sf-900 II SFM media (Thermo Fisher Scientific). All cells were routinely tested for mycoplasma contamination and were not authenticated after purchase.

CRISPR/Cas9-mediated genome editing
Gene editing for creation of KIF1C cells was performed as described previously (Ran et al., 2013). Briefly, in vitro–transcribed 20-nucleotide Alt-R CRISPR RNA (CrRNA, Hs.Cas9.KIF1C.1.AD) and Alt-R CRISPR/Cas9 trans-activating CRISPR RNA (tracrRNA) were purchased from Integrated DNA Technologies. The KIF1C exon 3 crRNA sequence was 5′-TCTCACTAACGCGAGAGAAG-3′. To prepare the Alt-R crRNA and Alt-R tracrRNA duplex, reconstituted oligos (100 μM) were mixed at equimolar concentrations in sterile PCR water and annealed at 95°C for 5 min, followed by slow cooling to room temperature. To generate knockout cells, 200 ng of pX459 vector and KIF1C crRNA-tracrRNA duplex (10 nM) were diluted in OptiMEM (Gibco) and combined with 1 μg/μl polyethylenimine (PEI; Polysciences Inc.) in a 4:1 ratio of PEI:DNA for transfection into 293T cells. 48 h after transfection, the cells were pulsed with 1 μg/ml puromycin for 24 h to allow selection of pX459-transfected cells. Following puromycin selection and recovery in DMEM without puromycin, single-cell clones were plated in 96-well format by limiting dilution and cultured to allow single colonies to grow out. Clones were expanded to 12-well plates, and samples of resulting clones were screened via immunoblotting with two independent gene-specific antibodies (KIF1C, rabbit polyclonal Novus No. NBP1-85978, immunogen from aa 996–1096, and rabbit polyclonal, Thermo Fisher Scientific No. PA5-27657, immunogen from aa 452–758). A SURVEYOR mutation detection kit (706020; Integrated DNA Technologies) was used to detect KIF1C-edited clones.

Stable cell lines with near-endogenous protein expression generation
KIF1C[KO] clones were reconstituted with near-endogenous KIF1C-BioID-3xFLAG, KIF1C-tagRFP-3xFLAG, or KIF1C[Δ794-807]-tagRFP-3xFLAG, respectively, using a retroviral infection/MSCV-driven expression system as described previously (Sowa et al., 2009). Briefly, plasmid DNA (retroviral pMSCV with KIF1C-3xFLAG-BioID, BioID-3xFLAG, KIF1C-tagRFP-3xFLAG, and KIF1C[Δ794-807]-tagRFP-3xFLAG genes inserted) along with viral helper constructs (retroviral MSCV-vsvg, MSCV-gag/pol) were diluted in OptiMEM (Gibco) and combined with 1 μg/μl PEI (Polysciences Inc.) in a 3:1 ratio of PEI:DNA concentration. The transfection mixture was added to 293T cells, followed by incubation for 12–16 h. Fresh DMEM was added to the cells, followed by a 24-h incubation to allow virus production. Viral supernatant was collected, filtered, and added to recipient 293T cells along with 1 μg/ml polybrene (Sigma-Aldrich) for infection. Stable cell lines were established by puromycin selection (0.75 μg/ml) for 48–72 h. Expression of exogenous proteins was confirmed via immunoblotting with anti-KIF1C and anti-FLAG M2-HRP antibodies.

FLP/FRT stable cell line generation
Dynein (IC2-SNAPf-3xFLAG), dynactin (p62-Halo-3xFLAG), kinesin (KIF1A, KIF1B, KIF1C, KIF5A, KIF5B, and KIF5C), carboxy-terminal BIoID-3xFLAG, and BioID-3xFLAG stable cell lines were created with the FLP/FRT system and T-Rex 293T cells (Invitrogen). These lines were generated as previously described (Redwine et al., 2017). Briefly, 1 d before transfection cells were plated onto 10-cm dishes. Cells were transfected with 30 μl of Lipofectamine 2000 and a combination of the appropriate pcDNA5/FRT/GOI construct and Flipase-expressing pOG44 plasmid (5 μg of total DNA: nine parts pOG44 + one part pcDNA5/FRT/GOI). After a 24-h recovery, cells were grown in DMEM containing 10% FBS, 1% PenStrep, and 50 μg/ml Hygromycin B. Colonies were isolated, expanded, and screened for expression of the fusion proteins by immunoblotting with an anti-FLAG M2-HRP antibody.

Transient transfections
For small-scale immunoprecipitations from transiently transfected 293T cells, 1.5×10^6 cells were plated onto a 10-cm dish 1 d before transfection. Transfections were performed with PEI and 2 μg of transfection-grade DNA (Purelink midi prep kit; Invitrogen) per dish, with the exception of Halo-Hook3[NT]-3xFLAG, where 1 μg of DNA was used due to high-protein expression if higher amounts of DNA were used. After 24 h, the media was exchanged to fresh DMEM containing 10% FBS and 1% PenStrep. Cells were then grown for an additional 24 h before lysate preparation. For large-scale protein purifications, 293T cells were plated onto 30 × 15-cm dishes and grown to ~50% confluence. Cells were transiently transfected with PEI and 7.5 μg DNA per plate. The PEI/DNA mixture was added to plates containing fresh DMEM + 10% FBS (no antibiotics) and incubated overnight. The following day, the cells were split 1:3 into 90 × 15-cm plates and incubated an additional 24 h. Cells were collected by pipetting with ice-cold 1×

Kendrick et al.
Hook3 is a scaffold for opposite-polarity motors

Journal of Cell Biology
https://doi.org/10.1083/jcb.201812170

2993

PBS, pH 7.4, centrifuged, and washed twice with 1× PBS. The cells were flash-frozen in liquid nitrogen before lysis.

For immunofluorescence, 0.01–0.03 × 10⁶ cells were plated onto fibronectin (0.001%; Sigma-Aldrich) coated glass coverslips in 24-well plates and grown for 24 h. The next day, transfections were performed with Lipofectamine 2000 and 0.5 µg DNA per well. The Lipofectamine/DNA mixture was added to wells containing fresh DMEM + 10% FBS (no antibiotics) and incubated overnight. The following day, cells were fixed and stained.

Immunoprecipitations

Immunoprecipitation from transiently transfected cells
Transiently transfected cells were collected by decanting the media and washing the cells off the dish with ice-cold 1× PBS. Cells were collected by centrifugation at 1,000 × g for 3 min, washed again with 1× PBS, and then transferred with 1× PBS to Eppendorf tubes for lysis. After spinning at 2,000 rpm in a microcentrifuge for 4 min and removing the 1× PBS, cells were flash-frozen for storage or immediately lysed in 500 µl of dynein lysis buffer (DLB; 30 mM Hepes, pH 7.4, 50 mM KOAc, 2 mM MgOAc, 1 mM EGTA, pH 7.5, and 10% glycerol) supplemented with 1 mM DTT, 0.2% Triton X-100, and 1× protease inhibitor cocktail (cOmplete Protease Inhibitor Cocktail; Roche) with gentle mixing at 4°C for 20 min. Lysates were then centrifuged at maximum speed in a 4°C microcentrifuge for 15 min. For each immunoprecipitation, 420 µl clarified lysate was retrieved and added to 50 µl packed volume of anti-FLAG M2 agarose slurry (Sigma-Aldrich) and incubated for 2 h at 4°C. Cells were washed four times with 1 ml of DLB, and elutions were performed with 50 µl of DLB supplemented with 1 mg/ml 3xFLAG peptide (ApexBio).

Immunoprecipitation of endogenous proteins
Wild-type 293T cells were grown to ~75% confluence and collected by pipetting with cold 1× PBS on ice. For each immunoprecipitation, a single 15-cm plate was collected, washed, and resuspended in 1 ml of DLB supplemented with 1 mM DTT, 0.2% Triton X-100, and 1× protease inhibitor cocktail (cOmplete Protease Inhibitor Cocktail; Roche). Resuspended cells were gently mixed at 4°C for 15 min, and then centrifuged at maximum speed in a 4°C microcentrifuge. The beads were prepared by incubating appropriate antibodies with Dynabeads Protein G (Thermo Fisher Scientific). For each immunoprecipitation sample, 100 µl of bead slurry was washed three times with 500 µl of 1× PBS and then resuspended in 100 µl of 1× PBS. To this mixture, 4 µg of the appropriate antibody was added (Hook3; ProteinTech No. 15457–1-AP, immunogen full-length protein; KIF1C, Bethyl No. A301-070A, immunogen from aa 900–950; Normal Rabbit IgG, Cell Signaling Technology No. 2729) and incubated for 30 min at room temperature. The resin was washed twice with 1× PBS and then once with DLB. After removing the final wash, 1 ml of cell lysate was added to the prepared resin and incubated for 4 h at 4°C. The beads were then washed three times with 1 ml DLB. To elute proteins, the resin was resuspended in 60 µl of 4× sample buffer and heated at 95°C

for 5 min. Eluted proteins were analyzed by SDS-PAGE followed by immunoblotting.

Immunoblotting and antibodies
Lysates and eluates were run on 4–15% polyacrylamide gels (NuPage; Invitrogen). Protein gels were transferred to polyvinylidene difluoride membranes for 1.5 h at 110 V (constant voltage) at 4°C. The membranes were blocked with PBS + 0.05% Tween-20 (vol/vol) + 5% dry milk (wt/vol) and immunoblotted with the appropriate antibodies. All antibodies were diluted in PBS + 0.05% Tween-20 + 1% milk (wt/vol). Primary antibodies were incubated overnight at 4°C, while secondary antibodies were incubated for 1 h at room temperature. Immunoblots were visualized with Supersignal West Pico Chemiluminescent reagent (Thermo Fisher Scientific) or Supersignal West Femto Chemiluminescent reagent (Thermo Fisher Scientific) on a VersaDoc imaging system (BioRad). Image intensity histograms were adjusted in Image Laboratory Version 6.0.1 (BioRad) and then imported into Adobe Illustrator to make figures.

Antibodies used for immunoblots were as follows: anti-FLAG M2-HRP (Sigma-Aldrich No. A8592; 1:5,000 dilution), anti-KIF1C (Novus Biotechnologies No. NBP1-85978, immunogen from aa 996–1096;1:500 dilution), anti-actin (Thermo Fisher Scientific No. MAP-15739, immunogen: β-actin amino-terminal peptide; 1:4,000 dilution), anti-Hook3 (ProteinTech No. 15457–1-A, immunogen: full-length protein; 1:1,000 dilution), goat anti-rabbit HRP (Santa Cruz Biotechnology No. sc-2030; 1:4,000 dilution) and goat anti-mouse HRP (Santa Cruz Biotechnology No. sc-2031; 1:4,000 dilution).

Immunofluorescence, confocal microscopy and image analysis
Fixation and staining
Cells of each condition were grown on fibronectin-coated glass coverslips, transfected if indicated, and fixed with 4% PFA (Thermo Fisher Scientific) in 1× PBS. Cells were washed with PBS, then permeabilized and blocked with 5% normal goat serum (Cell Signaling Technology) in PBS containing 0.5% Triton X-100 (Sigma-Aldrich). Cells were immunostained overnight at 4°C with indicated antibodies diluted in PBS with 1% BSA (Sigma-Aldrich) and 0.1% Triton X-100. The following day, cells were washed with PBS and stained with appropriate secondary antibodies and Alexa Fluor 647– or 488–conjugated phalloidin (Invitrogen). Cells were then washed with PBS, and coverslips were mounted on glass slides with CitiFluor AF1 mounting media (TedPella).

Antibodies used for immunofluorescence were as follows: anti-Hook3 (Thermos Fisher Scientific No. PA5-55172, immunogen full-length protein; 1:200 dilution), anti-dynactin (p150, BD Bioscience No. 610473, immunogen from aa 3–202; 1:200 dilution), anti-V5 (Sigma-Aldrich, No. V8137; 1:1,000 dilution), goat anti-rabbit IgG (H+L) Alexa Fluor 568 (Thermo Fisher Scientific No. A11036; 1:500 dilution), goat anti-rabbit IgG (H+L) Alexa Fluor 488 (Thermo Fisher Scientific No. A11008; 1:500 dilution), and goat anti-mouse IgG (H+L) Alexa Fluor 647 (Thermo Fisher Scientific No. A28181; 1:500 dilution).

Confocal microscopy

Cells were imaged using a Nikon A1R HD confocal microscope with a four-line (405 nm, 488 nm, 561 nm, and 640 nm) LUN-V laser engine and DU4 detector using bandpass and longpass filters for each channel (450/50, 525/50, 595/50, and 700/75), mounted on a Nikon Ti2 using an Apo 100× 1.49 NA objective. Image stacks were acquired in resonant mode with bidirectional scanning and 2× or 4× line averaging. The lasers used were 405 nm, 488 nm, 561 nm, and 640 nm. To avoid cross-talk between channels, z-stacks were acquired of the AlexaFluor 568 or tagRFP channel first, and the sfGFP or Alexa Fluor 488 and Alexa Fluor 647 channels were acquired subsequently. Illumination and image acquisition was controlled by NIS Elements Advanced Research software (Nikon Instruments).

Quantification of colocalization between KIF1C, Hook3, and dynactin

The colocalization with KIF1C was measured with a multi-step automated script assembled with the GA3 module within NIS Elements (Nikon Instruments). In the first step, an intensity and size threshold using the phalloidin or sfGFP channel was used to map the area of the intracellular region. The intracellular region was defined as all cells within the image containing KIF1C signal. Then KIF1C-positive foci were identified by applying a second threshold in the red channel based on fluorescence intensity and size. Binary masks of the KIF1C-positive foci that were within the intracellular masks were selected, and the intensity of Hook3 or dynactin staining within the KIF1C foci and intracellular binaries was measured. The average intensity of Hook3 or dynactin under the KIF1C mask was then divided by the average intensity of Hook3 or dynactin under the intracellular mask. This normalized fluorescence intensity of Hook3 or dynactin contained within the foci was then plotted for each condition. For each condition, ≥30 cells were analyzed per experiment. Data visualization and statistical analysis were performed using GraphPad Prism (8.0d; GraphPad Software). Statistical analysis was performed with unpaired t test and one-way ANOVA with Tukey post-test. Maximum projection images of confocal z-stacks and plot profiles of 15 µm lines drawn through individual z-sections were generated in ImageJ (2.0) and imported into Adobe Illustrator (version 21.0.1) to make figures. Brightness and contrast of all representative images were adjusted in ImageJ.

BioID sample preparation and MS
Cell growth and streptavidin purification

Growth of cells and sample preparation for BioID experiments were performed as previously described with slight modifications (Redwine et al., 2017). Briefly, BioID-3xFLAG or KIF1C-BioID-3xFLAG cells were plated at ~20% confluence in 15-cm dishes as four replicates, with each replicate consisting of 8 × 15-cm plates. After 24 h, biotin was added to the media to a final concentration of 50 µM, and the cells were allowed to grow for another 16 h. After decanting the media, cells were dislodged from each plate by pipetting with ice-cold 1× PBS. Cells were centrifuged at 1,000 × g for 2 min followed by two washes with ice-cold 1× PBS, and the cell pellets were resuspended and lysed in 16 ml RIPA buffer (50 mM Tris-HCl, pH 8.0, 150 mM NaCl, 1% [vol/vol] NP-40, 0.5% [wt/vol] sodium deoxycholate, 0.1% [wt/vol] SDS, 1 mM DTT, and protease inhibitors [cOmplete Protease Inhibitor Cocktail; Roche]) by gentle rocking for 15 min at 4°C. The cell lysate was clarified via centrifugation at 66,000 × g for 30 min in a Ti70 rotor (Beckman Coulter) at 4°C. The clarified lysate was retrieved and combined with prewashed 0.8 ml streptavidin-conjugated beads (Pierce Streptavidin magnetic beads) and incubated overnight at 4°C with gentle rocking. Bead/lysate mixtures were collected on a magnetic stand into a single 2-ml round-bottom microcentrifuge tube. The beads were then washed three times with 2-ml RIPA buffer and once with 1× PBS with immobilization and solution removal performed on a magnetic stand.

On-bead digestion

Samples were prepared for MS as follows. After the final wash, the beads were resuspended in 100 µl of 50 mM ammonium bicarbonate (Thermo Fisher Scientific), and the proteins on the beads were reduced with 10 mM DTT for 30 min at room temperature and alkylated with 55 mM iodoacetamide (Sigma-Aldrich) for 30 min in the dark. Protein digestion was performed with sequencing grade modified trypsin (Promega) at 1/50 protease/protein (wt/wt) at 37°C overnight. After trypsin digestion, the beads were washed twice with 100 µl of 80% acetonitrile (Thermo Fisher Scientific) in 1% formic acid (Thermo Fisher Scientific), and the supernatants were collected. Samples were dried in Speed-Vac (Thermo Fisher Scientific) and desalted and concentrated on a C18 Tip (Thermo Fisher Scientific).

MS data acquisition

On-bead digested samples were analyzed on an Orbitrap Fusion mass spectrometer (Thermo Fisher Scientific) coupled to an Easy-nLC 1200 system (Thermo Fisher Scientific) through a nanoelectrospray ion source. Peptides were separated on a self-made C18 analytical column (100 µm internal diameter × 20 cm length) packed with 2.7 µm Cortecs particles. After equilibration with 3 µl 5% acetonitrile and 0.1% formic acid mixture, the peptides were separated by a 120-min linear gradient from 6 to 42% acetonitrile with 0.1% formic acid at 400 nl/min. Liquid chromatography (Optima LC/MS; Thermo Fisher Scientific) mobile phase solvents and sample dilutions were all made in 0.1% formic acid diluted in water (buffer A) and 0.1% formic acid in 80% acetonitrile (buffer B). Data acquisition was performed using the instrument-supplied Xcalibur (version 4.1) software. Survey scans covering the mass range of 350–1,800 were performed in the Orbitrap by scanning from a mass/charge ratio (m/z) of 300–1800 with a resolution of 120,000 (at m/z 200), an S-Lens RF Level of 30%, a maximum injection time of 50 ms, and an automatic gain control target value of 4 × 10⁵. For MS2 scan triggering, monoisotopic precursor selectfon was enabled, charge state filtering was limited to 2–7, an intensity threshold of 2 × 10⁴ was used, and dynamic exclusion of previously selected masses was enabled for 45 s with a tolerance of 10 ppm. MS2

scans were acquired in the Orbitrap mode with a maximum injection time of 35 ms, quadrupole isolation, an isolation window of 1.6 m/z, higher-energy collisional dissociation of 30%, and an automatic gain control target value of 5×10^4.

MS data analysis
MS/MS spectra were extracted from raw data files and converted into .mgf files using a Proteome Discoverer Software (version 2.1.0.62). These .mgf files were then independently searched against human database using an in-house Mascot server (version 2.6; Matrix Science). Mass tolerances were ±10 ppm for MS peaks, and ±25 ppm for MS/MS fragment ions. Trypsin specificity was used, allowing for one missed cleavage. Met oxidation, protein amino-terminal acetylation, amino-terminal biotinylation, lysine biotinylation, and peptide amino-terminal pyroglutamic acid formation were allowed as variable modifications, while carbamidomethyl of Cys was set as a fixed modification. Scaffold (version 4.8; Proteome Software) was used to validate MS/MS-based peptide and protein identifications. Peptide identifications were accepted if they could be established at >95.0% probability as specified by the Peptide Prophet algorithm. Protein identifications were accepted if they could be established at >99.0% probability and contained at least two identified unique peptides.

To estimate relative protein levels, distributed normalized spectral abundance factors (dNSAFs) were calculated for each nonredundant protein, as described previously (Zhang et al., 2010). Average dNSAFs were calculated for each protein using replicates with nonzero dNSAF values. Enrichment of proteins in streptavidin affinity purifications from KIF1C-BioID-3xFLAG–tagged stable cell line relative to a control BioID stable cell line was calculated for all replicates as the ratio of average dNSAF (ratio = average dNSAF$_{\text{KIF1C-BioID}}$:average dNSAF$_{\text{BioID}}$). The volcano plot (Fig. 1 D) was generated by plotting the log$_2$(fold enrichment) against the –log$_{10}$(P value), where the P value (two-tailed Student's t test) was computed by comparing the replicate dNSAF values of KIF1C-BioID to the BioID control. Potential KIF1C interactions were included as significant if they were not present in the control samples or were more than threefold enriched in the KIF1C-BioID-3xFLAG dataset and had P values <0.05.

Protein purification
KIF1C
Different KIF1C constructs were purified from 293T cells transiently transfected with KIF1C-SNAPf-3xFLAG or KIF1C$^{\Delta794\text{-}807}$-SNAPf-3xFLAG. Frozen cell pellets from 45 plates were resuspended in 60 ml of BRB80 lysis buffer (80 mM Pipes, pH 6.8, 1 mM MgCl$_2$, 1 mM EGTA, 10% glycerol, and 50 mM KOAc) supplemented with 1 mM DTT, 0.5 mM ATP, 0.2% Triton X-100, and 1× protease inhibitor cocktail [cOmplete Protease Inhibitor Cocktail; Roche]) and gently mixed at 4°C for 15 min. The lysed cells were then centrifuged at 30,000 rpm in a Ti70 rotor (Beckman Coulter) at 4°C for 30 min. The clarified lysate was retrieved and added to 0.7 ml packed anti-FLAG M2 agarose resin (Sigma-Aldrich) and incubated with gentle mixing at 4°C for 16 h. After incubation, the lysate/resin mixture was

centrifuged at 1,000 rpm for 2 min at 4°C to pellet the resin, the supernatant was decanted, and the resin was transferred to a column at 4°C. The column was washed with 50 ml low-salt wash buffer (80 mM Pipes, pH 6.8, 1 mM MgCl$_2$, 1 mM EGTA, 10% glycerol, 50 mM KOAc, 1 mM DTT, 0.02% Triton X-100, and 0.5 mM Pefabloc), 100 ml high-salt wash buffer (80 mM Pipes, pH 6.8, 1 mM MgCl$_2$, 1 mM EGTA, 10% glycerol, 250 mM KOAc, 1 mM DTT, 0.02% Triton X-100, and 0.5 mM Pefabloc), and finally 150 ml low-salt wash buffer. After the final wash, the resin was resuspended in an equal volume of low-salt wash buffer (700 µl) and moved to room temperature, and 7 µl of SNAP-TMR (Promega) was added and mixed. The mixture was incubated in the dark at room temperature for 10 min. The column was returned to 4°C and washed with 100 ml of low-salt wash buffer. The labeling steps were omitted when unlabeled protein was desired. The resin was resuspended in 700 µl of low-salt wash buffer containing 2 mg/ml 3xFLAG peptide (ApexBio) and incubated for 30 min at 4°C. The purified protein was concentrated using a 100-kD molecular weight cut-off (MWCO) centrifugal filter (Amicon Ultra; Millipore). Each purified KIF1C construct was aliquoted, and aliquots were snap-frozen in liquid N$_2$ and stored at –80°C. Protein purity was determined on Sypro (Thermo Fisher Scientific)–stained SDS-PAGE gels. The labeling efficiency of KIF1C-SNAPf-TMR was 86% and of KIF1C$^{\Delta794\text{-}807}$-SNAPf-TMR was 99%.

Full-length Hook3
Full-length wild-type Hook3 (Halo-Hook3[1–718]-3xFLAG) was purified from transiently transfected 293T cells. Frozen cells (90 × 15-cm plates) were resuspended in 80 ml of DLB buffer supplemented with 1 mM DTT, 0.5 mM ATP, 0.2% Triton X-100, and 1× protease inhibitor cocktail (cOmplete Protease Inhibitor Cocktail; Roche) and gently mixed at 4°C for 15 min. The lysed cells were then centrifuged at 30,000 rpm in a Ti70 rotor (Beckman Coulter) at 4°C for 30 min. The clarified lysate was retrieved and added to 1.5 ml packed anti-FLAG M2 agarose (Sigma-Aldrich) and incubated with gentle mixing at 4°C for 16 h. After incubation, the lysate/resin mixture was centrifuged at 1,000 rpm for 2 min at 4°C to pellet the resin, the supernatant was decanted, and the resin was transferred to a column at 4°C. The column was washed with 100 ml low-salt wash buffer (30 mM Hepes, pH 7.4, 50 mM KOAc, 2 mM MgOAc, 1 mM EGTA, pH 7.5, 10% glycerol, 1 mM DTT, 0.5 mM ATP, 0.5 mM Pefabloc, and 0.02% Triton X-100), 100 ml high-salt wash buffer (30 mM Hepes, pH 7.4, 250 mM KOAc, 2 mM MgOAc, 1 mM EGTA, pH 7.5, 10% glycerol, 1 mM DTT, 0.5 mM ATP, 0.5 mM Pefabloc, and 0.02% Triton X-100), and finally with 100 ml low-salt wash buffer. The resin was then resuspended in an equal volume of low-salt wash buffer (1.5 ml), and 20 µl of 1 mM Halo–Alexa Fluor 488 was added and mixed. The mixture was incubated in the dark at room temperature for 10 min. The column was returned to 4°C and washed with 100 ml of low-salt wash buffer. The resin was resuspended in 1,000 µl of low-salt wash buffer containing 2 mg/ml 3xFLAG peptide (ApexBio) and incubated for 30 min at 4°C. The mixture was retrieved and centrifuged through a small filter column to remove the resin. The eluate was retrieved, and 500 µl was loaded onto a Superose

Kendrick et al.
Hook3 is a scaffold for opposite-polarity motors

Journal of Cell Biology 2996
https://doi.org/10.1083/jcb.201812170

6 Increase 10/300 GL Column connected to an AKTA FPLC (GE Healthcare) and run in "GF150" buffer (25 mM Hepes, pH 7.4, 150 mM KCl, 1 mM MgCl$_2$, and 1 mM DTT). Peak fractions containing Alexa Fluor 488–labeled Halo-Hook3-3xFLAG were pooled and concentrated, and buffer was exchanged to GF150 + 10% glycerol using a 100-kD MWCO centrifugal filter (Amicon Ultra; Millipore). Aliquots were snap-frozen in liquid N$_2$ and stored at –80°C. Protein purity was checked on a Sypro (Thermo Fisher Scientific)–stained SDS-PAGE gel. The labeling efficiency was 91%.

Hook3^{Hook2} chimera

Hook3^{Hook2} chimera (ZZ-TEV-Halo-Hook3[1–552]-Hook2[548–719]) was purified from baculovirus-infected Sf9 insect cells. Cell pellets from 800 ml culture were resuspended in DLB supplemented with 0.5 mM ATP, 0.2% Triton X-100, 300 mM KOAc, and 1× protease inhibitor cocktail (cOmplete Protease Inhibitor Cocktail; Roche) and lysed using a Dounce homogenizer (15 strokes with loose plunger and 10 strokes with tight plunger). The lysate was clarified by centrifuging at 183,960 × g for 30 min. The clarified lysate was retrieved and added to 1.5 ml of IgG Sepharose 6 Fast Flow affinity resin (GE Healthcare), preequilibrated in DLB buffer, and incubated with gentle mixing at 4°C for 2 h. After incubation, the lysate/resin mixture was centrifuged at 1,000 rpm for 2 min at 4°C to pellet the resin, the supernatant was decanted, and the resin was transferred to a column at 4°C. The column was washed with 100 ml low-salt TEV buffer (10 mM Tris-HCl, pH 8, 2 mM MgOAc, 1 mM EGTA, pH 7.5, 10% glycerol, 1 mM DTT, and 250 mM KOAc), 100 ml high-salt TEV buffer (10 mM Tris-HCl, pH 8, 2 mM MgOAc, 1 mM EGTA, pH 7.5, 10% glycerol, 1 mM DTT, and 500 mM KOAc), and finally 100 ml low-salt TEV buffer. The resin was then resuspended in an equal volume of low-salt TEV buffer supplemented with 0.02% NP-40 and TEV protease and incubated ~16 h followed by labeling with 20 μl of 1 mM Halo–Alexa Fluor 488. The mixture was incubated at 4°C in the dark for 2 h. After labeling, the mixture was retrieved and centrifuged through a small filter column to remove the resin. The eluate was retrieved, and 500 μl was loaded onto a Superose 6 Increase 10/300 GL Column connected to an AKTA FPLC (GE Healthcare) and run in GF150 buffer. Peak fractions containing Alexa Fluor 488–labeled Halo-Hook3^{Hook2}-3xFLAG were pooled and concentrated, and buffer was exchanged to GF150 + 10% glycerol using a 100-kD MWCO centrifugal filter (Amicon Ultra; Millipore). Aliquots were snap-frozen in liquid N$_2$ and stored at –80°C. Protein purity was checked on a Sypro (Thermo Fisher Scientific)-stained SDS-PAGE gel. The labeling efficiency was 94%.

Hook3^{NT}

The Hook3^{NT} (Strep-Halo-Hook3[1–552]) construct was transformed into BL21-CodonPlus (DE3)-RIPL cells (Agilent). 2 liters of cells were grown at 37°C in LB media to a 600-nm optical density of 0.4–0.8 before the temperature was reduced to 18°C and expression was induced with 0.5 mM IPTG. After 16–18 h, the cells were harvested via centrifugation for 6 min at 4°C at 6,000 rpm in a Beckman Coulter JLA 8.1000 fixed-angle rotor. Pellets were resuspended in 40 ml of DLB supplemented with 0.5 mM Pefabloc SC (Sigma-Aldrich) and 1 mg/ml lysozyme and incubated at 4°C for 30 min. Cells were lysed via sonication

(Branson Digital Sonifier) and clarified via centrifugation at 66,000 × g for 30 min in a Ti70 rotor (Beckman Coulter) at 4°C. Supernatant was loaded onto a 5-ml StrepTrap column (GE Healthcare) and washed with 50–100 ml of lysis buffer. Strep-Halo-Hook3^{NT} was eluted with 25–50 ml of elution buffer (DLB with 3 mM d-Desthiobiotin). Elution was then applied to a size exclusion chromatography Superose 6 Increase 10/300 GL column (GE Healthcare) that had been equilibrated with GF150 buffer. Peak fractions containing Alexa Fluor 488 Strep-Halo-Hook3^{NT} were pooled and concentrated using a 100-kD MWCO centrifugal filter (Amicon Ultra; Millipore). Aliquots were snap-frozen in liquid N$_2$ and stored at –80°C. Protein purity was assayed by SDS-PGAE and Sypro (Thermo Fisher Scientific) staining. The labeling efficiency was 75%.

Dynein and dynactin

Dynein (IC2-SNAPf-3xFLAG) and dynactin (p62-Halo-3xFLAG) were purified from stable cell line as previously described (Redwine et al., 2017). Briefly, frozen pellets from 293T cells (80 × 15-cm plates, dynein and 160 × 15-cm plates, dynactin) were resuspended in DLB supplemented with 0.5 mM ATP, 0.2% Triton X-100, and 1× protease inhibitor cocktail (cOmplete Protease Inhibitor Cocktail; Roche) and gently mixed at 4°C for 15 min. The lysed cells were then centrifuged at 30,000 rpm in a Ti70 rotor (Beckman Coulter) at 4°C for 30 min. The clarified lysate was retrieved and added to 1.5 ml (dynein) or 3 ml (dynactin) of packed anti-FLAG M2 agarose resin (Sigma-Aldrich) and incubated with gentle mixing at 4°C for 16 h. After incubation, the lysate/resin mixture was centrifuged at 1,000 rpm for 2 min at 4°C to pellet the resin, and the supernatant was decanted. The resin was transferred to a column at 4°C, and the column was washed with 100 ml low-salt wash buffer (30 mM Hepes, pH 7.4, 50 mM KOAc, 2 mM MgOAc, 1 mM EGTA, pH 7.5, 10% glycerol, 1 mM DTT, 0.5 mM ATP, 0.5 mM Pefabloc, and 0.02% Triton X-100), 100 ml high-salt wash buffer (30 mM Hepes, pH 7.4, 250 mM KOAc, 2 mM MgOAc, 1 mM EGTA, pH 7.5, 10% glycerol, 1 mM DTT, 0.5 mM ATP, 0.5 mM Pefabloc, and 0.02% Triton X-100), and finally 50 ml low-salt wash buffer. After the final wash, the resin was resuspended in an equal volume of low-salt wash buffer and moved to room temperature, and 15 μl of 1 mM SNAP–Alexa Fluor 647 was added and mixed. The mixture was incubated in the dark at room temperature for 10 min. The column was returned to 4°C and washed with 100 ml of low-salt wash buffer. The labeling steps were omitted when unlabeled protein was desired. The resin was resuspended in 800 μl of low-salt wash buffer containing 2 mg/ml 3xFLAG peptide (ApexBio) and incubated for 30 min at 4°C. The mixture was retrieved and centrifuged through a small filter column to remove the resin. The eluate was next loaded onto a Mono Q 5/50 GL 1-ml column on an AKTA FPLC (GE Healthcare). The column was washed with 5 ml buffer A (50 mM Tris-HCl, pH 8.0, 2 mM MgOAc, 1 mM EGTA, and 1 mM DTT) and then subjected to a 26-ml linear gradient from 35–100% buffer B mixed with buffer A (buffer B = 50 mM Tris-HCl, pH 8.0, 1 M KOAc, 2 mM MgOAc, 1 mM EGTA, and 1 mM DTT), followed by 5 ml additional 100% buffer B. Fractions containing pure dynein (~60–70% Buffer B)

or pure dynactin (~75–80% buffer B) were pooled, and buffer was exchanged through iterative rounds of dilution and concentration on a 100-kD MWCO centrifugal filter (Amicon Ultra; Millipore) using GF150 buffer with 10% glycerol. Purity was evaluated on SDS-PAGE gels, and protein aliquots were snap-frozen in liquid N_2 and stored at –80°C. The labeling efficiency of dynein–Alexa Fluor 647 was 97%.

Microtubule preparation

Microtubules were polymerized from tubulin prepared from bovine brain as previously described (Waterman-Storer, 2001). Purified tubulin was labeled with Alexa Fluor 405 NHS Ester (Thermo Fisher Scientific), Alexa Fluor 488 NHS Ester (Thermo Fisher Scientific), N-ethylmaleimide (Thermo Fisher Scientific), or biotin ester (biotin-X; Thermo Fisher Scientific) by a series of polymerization and depolymerization steps. To make biotinylated Alexa Fluor 405 or Alexa Fluor 488 microtubules, fluorophore-labeled tubulin (10 μM) was mixed with biotin-tubulin (10 μM) and unlabeled tubulin (10 μM). The tubulin mixture was incubated on ice for 10 min followed by an addition of an equal volume of polymerization buffer (2× BRB80 supplemented with 2 mM DTT, 2 mM MgGTP, and 20% DMSO) and incubation for 30 min at 37°C. After incubation, an equal volume of BRB80 supplemented with 1 mM DTT and 20 μM taxol was added to the mixture, and microtubules were incubated for an additional 10 min at 37°C. Microtubules were used for up to 2 wk after polymerization and diluted 1:150–1:200 before single-molecule assays.

Polarity-marked microtubules were prepared according to a previously described protocol with slight modifications (Roberts et al., 2014). Brightly labeled, biotinylated microtubule seeds were polymerized by mixing Alexa Fluor 405–tubulin (10 μM), biotin-tubulin (10 μM), and unlabeled tubulin (10 μM) with 0.5 mM guanylyl-(α,β)-methylene diphosphonate (GMP-CPP; Jena Bioscience) in BRB80 supplemented with 1 mM DTT and incubating for 30 min at 37°C. Following the addition of 10× volume of BRB80, polymerized seeds were pelleted in a benchtop centrifuge (15 min at 16,100 × g) and resuspended in a volume of BRB80 equal to the original polymerization volume. GMP-CPP seeds were then mixed with 1:5 diluted dim mix containing 12 μM 405-tubulin, 15 μM unlabeled tubulin, 10 μM biotin-tubulin, and 15 μM N-ethylmaleimide–tubulin and incubated for 30 min at 37°C. After incubation, an equal volume of BRB80 supplemented with 1 mM DTT and 20 μM taxol was added to the mixture, and microtubules were incubated for additional 30 min at 37°C to generate polarity-marked microtubules. 1:25 diluted polarity-marked microtubules were flowed into flow chambers, and single-molecule motility analyses were performed as described below.

TIRF microscopy

Imaging was performed with an inverted microscope (Ti-E Eclipse; Nikon) equipped with a 100× 1.49 NA oil immersion objective (Plano Apo; Nikon). The xy position of the stage was controlled by ProScan linear motor stage controller (Prior). The microscope was equipped with an MLC400B laser launch (Agilent) equipped with 405-nm (30 mW), 488-nm (90 mW), 561-nm (90 mW), and 640-nm (170 mW) laser lines. The excitation and emission paths were filtered using appropriate single bandpass filter cubes (Chroma). The emitted signals were detected with an electron multiplying charge coupled device camera (iXon Ultra 888; Andor Technology). Illumination and image acquisition were controlled by NIS Elements Advanced Research software (Nikon).

Single-molecule motility assays

Single-molecule motility assays were performed in flow chambers using the TIRF microscopy setup described above. Biotinylated and PEGylated coverslips (Microsurfaces) were used to reduce nonspecific binding. Microtubules contained ~10% biotin-tubulin for attachment to a streptavidin-coated coverslip and ~10% Alexa Fluor 405 or 488 (Thermo Fisher Scientific) tubulin for visualization. Imaging buffer was DLB supplemented with 20 μM taxol, 1 mg/ml casein, 1 mM Mg-ATP, 71.5 mM β mercaptoethanol, an oxygen scavenger system, 0.4% glucose, 45 μg/ml glucose catalase (Sigma-Aldrich), and 1.15 mg/ml glucose oxidase (Sigma-Aldrich). Images were recorded every 0.3–0.4 s for 3 min. Movies showing significant drift were not analyzed.

For two-color motility assays of KIF1C with Hook3, 1.125 nM KIF1C-SNAPf-AlexaTMR was mixed with 2.25 nM Hook3–Alexa Fluor 488 or 2.25 nM Hook3[Hook2]–Alexa Fluor 488. The two-color motility measurements of dynein, dynactin, and different Hook3 constructs were all performed with 450 pM dynein–Alexa Fluor 647, 900 pM unlabeled dynactin, and 3.25 pM Hook3 (Hook3[NT]–Alexa Fluor 488, Hook3–Alexa Fluor 488, or Hook3[Hook2]–Alexa Fluor 488). The three-color single-molecule motility experiments were performed with 450 pM dynein–Alexa Fluor 647, 900 pM unlabeled dynactin, 130 nM Hook3 (Hook3–Alexa Fluor 488 or Hook3[Hook2]–Alexa Fluor 488), and 0.45 nM KIF1C (KIF1C-SNAPf-TMR or KIF1C[Δ794-807]-SNAPf-TMR). Two-color motility measurements with increasing concentrations of KIF1C were performed with 450 pM dynein–Alexa Fluor 647, 900 pM unlabeled dynactin, 3.25 pM Hook3, and the following concentrations of unlabeled KIF1C: 450 pM, 900 pM, or 1.8 nM. Each protein mixture was incubated on ice for 10 min before TIRF imaging. The order of protein addition or preincubation of Hook3 with KIF1C before dynein and dynactin addition did not affect complex behavior.

Bleaching analysis

Bleach step analysis was performed in a flow chamber as described above with biotin–Alexa Fluor 488 microtubules immobilized to the coverslips. 560 pM KIF1C-TMR in the presence or absence of 1.125 nM Hook3-488 was flowed into the chamber in the presence of DLB supplemented with 1 mM AMP-PNP (Sigma-Aldrich), 100 μM taxol, and 0.1 mg/ml casein. Images were acquired every 100 ms for 160 s using a 562-nm laser at 50% power. Images were analyzed in ImageJ with Plot Profile function. Steps were manually counted from individual spot profiles.

TIRF data analysis

The velocity of moving particles was calculated from kymographs generated in ImageJ as described previously (Roberts et al., 2014). Velocities were only calculated from molecules that moved processively for more than five frames. Nonmotile or diffusive events were not considered in velocity calculation. Processive events were defined as events that move unidirectionally and do not exhibit directional changes >600 nm. Diffusive events were defined as events that exhibit at least one bidirectional movement >600 nm in each direction. Single-molecule movements that change apparent behavior (e.g., shift from nonmotile to processive) were considered as multi-velocity events and counted as multiple events. For run length analysis, the length of each track in a multi-velocity event was combined to calculate total run length. Pausing frequency was calculated by measuring the number of pauses in multi-velocity events and dividing this number by the total run length of the multi-velocity event. Landing rates were calculated by counting the number of processive events that start after the first frame and end before the last frame of each movie and dividing this number by the microtubule length and total movie time.

Data visualization and statistical analyses were performed using GraphPad Prism (8.0d; GraphPad Software), Excel (version 16.20; Microsoft), XLSTAT (2019.1.3.; Addinsoft), and ImageJ (2.0). Brightness and contrast were adjusted in ImageJ for all videos and kymographs. In addition, images in Fig. 5 B were manually colored (yellow) in Photoshop (version 20; Photoshop CC) to highlight the three-color colocalized runs. For run length analysis, data were plotted as a 1-cumulative probability distribution and fit to a one-phase exponential decay function (least squares fit). Statistical analyses for velocities, pausing frequency, and landing rates were performed using an unpaired t test with Welch's correction. Errors for run length analysis of KIF1C and KIF1C/Hook3 were generated using a bootstrapping method (each run length value was resampled 200 times) and statistical significance was analyzed using an unpaired t test with Welch's correction. Statistical comparisons of the plus end and minus end moving events were performed using one-way ANOVA with Tukey post-test. The exact value of N and evaluation of statistical significance are described in the corresponding figures and figure legends. All experiments were analyzed from at least three independent replicates unless otherwise stated.

Sequence alignment

Protein sequences of different Hook isoforms were obtained from UniProt. Sequence alignments were performed with Clustal Omega web services (McWilliam et al., 2013) and annotated using Jalview (Biasini et al., 2014).

Online supplemental material

Fig. S1 shows the motile properties of KIF1C in the presence and absence of Hook3. Fig. S2 shows the mapping of the Hook3 and KIF1C interaction. Fig. S3 shows the motile properties of dynein in the presence of purified full-length Hook3, the Hook3 amino terminus, and a Hook3-Hook2 chimera. Fig. S4 shows that Hook3 scaffolds dynein and KIF1C for opposite polarity motility.

Fig. S5 shows that dynactin localization is unaffected by KIF1C expression. Video 1 shows the movement of KIF1C-TMR on 405-labeled microtubules. Video 2 shows the movement of KIF1C-TMR in the presence of Hook3-488 on 405-labeled microtubules. Video 3 shows the movement of KIF1C$^{\Delta794-807}$-TMR on 405-labeled microtubules. Video 4 shows the movement of KIF1C$^{\Delta794-807}$-TMR in the presence of Hook3-488 on 405-labeled microtubules. Video 5 shows the movement of KIF1C-TMR in the presence of Hook3^{Hook2}-488 on 405-labeled microtubules. Video 6 shows the movement of dynein-647, dynactin, and Hook3-488 on 405-labeled microtubules. Video 7 shows an example of a movement of dynein-647, dynactin, Hook3-488, and KIF1C-TMR on 405-labeled microtubules. Video 8 shows an example of a movement of dynein-647, dynactin, Hook3-488, and KIF1C-TMR on 405-labeled microtubules. Table S1 lists the MS results generated from the KIF1C-BioID experiment.

References

Abenza, J.F., A. Pantazopoulou, J.M. Rodríguez, A. Galindo, and M.A. Peñalva. 2009. Long-distance movement of Aspergillus nidulans early endosomes on microtubule tracks. *Traffic.* 10:57–75. https://doi.org/10.1111/j.1600-0854.2008.00848.x

Barkus, R.V., O. Klyachko, D. Horiuchi, B.J. Dickson, and W.M. Saxton. 2008. Identification of an axonal kinesin-3 motor for fast anterograde vesicle

transport that facilitates retrograde transport of neuropeptides. *Mol. Biol. Cell.* 19:274–283. https://doi.org/10.1091/mbc.e07-03-0261

Baumann, S., T. Pohlmann, M. Jungbluth, A. Brachmann, and M. Feldbrügge. 2012. Kinesin-3 and dynein mediate microtubule-dependent co-transport of mRNPs and endosomes. *J. Cell Sci.* 125:2740–2752. https://doi.org/10.1242/jcs.101212

Behrends, C., M.E. Sowa, S.P. Gygi, and J.W. Harper. 2010. Network organization of the human autophagy system. *Nature.* 466:68–76. https://doi.org/10.1038/nature09204

Belyy, V., M.A. Schlager, H. Foster, A.E. Reimer, A.P. Carter, and A. Yildiz. 2016. The mammalian dynein-dynactin complex is a strong opponent to kinesin in a tug-of-war competition. *Nat. Cell Biol.* 18:1018–1024. https://doi.org/10.1038/ncb3393

Biasini, M., S. Bienert, A. Waterhouse, K. Arnold, G. Studer, T. Schmidt, F. Kiefer, T. Gallo Cassarino, M. Bertoni, L. Bordoli, and T. Schwede. 2014. SWISS-MODEL: modelling protein tertiary and quaternary structure using evolutionary information. *Nucleic Acids Res.* 42(W1):W252-8. https://doi.org/10.1093/nar/gku340

Bielska, E., M. Schuster, Y. Roger, A. Berepiki, D.M. Soanes, N.J. Talbot, and G. Steinberg. 2014. Hook is an adapter that coordinates kinesin-3 and dynein cargo attachment on early endosomes. *J. Cell Biol.* 204:989–1007. https://doi.org/10.1083/jcb.201309022

Blasius, T.L., N. Reed, B.M. Slepchenko, and K.J. Verhey. 2013. Recycling of kinesin-1 motors by diffusion after transport. *PLoS One.* 8:e76081. https://doi.org/10.1371/journal.pone.0076081

Brendza, R.P., L.R. Serbus, W.M. Saxton, and J.B. Duffy. 2002. Posterior localization of dynein and dorsal-ventral axis formation depend on kinesin in Drosophila oocytes. *Curr. Biol.* 12:1541–1545. https://doi.org/10.1016/S0960-9822(02)01108-9

Carvalho, P., M.L. Gupta Jr., M.A. Hoyt, and D. Pellman. 2004. Cell cycle control of kinesin-mediated transport of Bik1 (CLIP-170) regulates microtubule stability and dynein activation. *Dev. Cell.* 6:815–829. https://doi.org/10.1016/j.devcel.2004.05.001

Derr, N.D., B.S. Goodman, R. Jungmann, A.E. Leschziner, W.M. Shih, and S.L. Reck-Peterson. 2012. Tug-of-war in motor protein ensembles revealed with a programmable DNA origami scaffold. *Science.* 338:662–665. https://doi.org/10.1126/science.1226734

DeSantis, M.E., M.A. Cianfrocco, Z.M. Htet, P.T. Tran, S.L. Reck-Peterson, and A.E. Leschziner. 2017. Lis1 Has Two Opposing Modes of Regulating Cytoplasmic Dynein. *Cell.* 170:1197–1208.e12. https://doi.org/10.1016/j.cell.2017.08.037

Dor, T., Y. Cinnamon, L. Raymond, A. Shaag, N. Bouslam, A. Bouhouche, M. Gaussen, V. Meyer, A. Durr, A. Brice, et al. 2014. KIF1C mutations in two families with hereditary spastic paraparesis and cerebellar dysfunction. *J. Med. Genet.* 51:137–142. https://doi.org/10.1136/jmedgenet-2013-102012

Dorner, C., T. Ciossek, S. Müller, P.H. Møller, A. Ullrich, and R. Lammers. 1998. Characterization of KIF1C, a new kinesin-like protein involved in vesicle transport from the Golgi apparatus to the endoplasmic reticulum. *J. Biol. Chem.* 273:20267–20275. https://doi.org/10.1074/jbc.273.32.20267

Efimova, N., A. Grimaldi, A. Bachmann, K. Frye, X. Zhu, A. Feoktistov, A. Straube, and I. Kaverina. 2014. Podosome-regulating kinesin KIF1C translocates to the cell periphery in a CLASP-dependent manner. *J. Cell Sci.* 127:5179–5188. https://doi.org/10.1242/jcs.149633

Egan, M.J., K. Tan, and S.L. Reck-Peterson. 2012. Lis1 is an initiation factor for dynein-driven organelle transport. *J. Cell Biol.* 197:971–982. https://doi.org/10.1083/jcb.201112101

Encalada, S.E., L. Szpankowski, C.-H. Xia, and L.S.B. Goldstein. 2011. Stable kinesin and dynein assemblies drive the axonal transport of mammalian prion protein vesicles. *Cell.* 144:551–565. https://doi.org/10.1016/j.cell.2011.01.021

Engelender, S., A.H. Sharp, V. Colomer, M.K. Tokito, A. Lanahan, P. Worley, E.L. Holzbaur, and C.A. Ross. 1997. Huntingtin-associated protein 1 (HAP1) interacts with the p150Glued subunit of dynactin. *Hum. Mol. Genet.* 6:2205–2212. https://doi.org/10.1093/hmg/6.13.2205

Farkhondeh, A., S. Niwa, Y. Takei, and N. Hirokawa. 2015. Characterizing KIF16B in neurons reveals a novel intramolecular "stalk inhibition" mechanism that regulates its capacity to potentiate the selective somatodendritic localization of early endosomes. *J. Neurosci.* 35:5067–5086. https://doi.org/10.1523/JNEUROSCI.4240-14.2015

Friedman, D.S., and R.D. Vale. 1999. Single-molecule analysis of kinesin motility reveals regulation by the cargo-binding tail domain. *Nat. Cell Biol.* 1:293–297. https://doi.org/10.1038/13008

Guimaraes, S.C., M. Schuster, E. Bielska, G. Dagdas, S. Kilaru, B.R.A. Meadows, M. Schrader, and G. Steinberg. 2015. Peroxisomes, lipid droplets, and endoplasmic reticulum "hitchhike" on motile early endosomes. *J. Cell Biol.* 211:945–954. https://doi.org/10.1083/jcb.201505086

Guo, X., G.G. Farías, R. Mattera, and J.S. Bonifacino. 2016. Rab5 and its effector FHF contribute to neuronal polarity through dynein-dependent retrieval of somatodendritic proteins from the axon. *Proc. Natl. Acad. Sci. USA.* 113:E5318–E5327. https://doi.org/10.1073/pnas.1601844113

Hackney, D.D., and M.F. Stock. 2000. Kinesin's IAK tail domain inhibits initial microtubule-stimulated ADP release. *Nat. Cell Biol.* 2:257–260. https://doi.org/10.1038/35010525

Hammond, J.W., D. Cai, T.L. Blasius, Z. Li, Y. Jiang, G.T. Jih, E. Meyhofer, and K.J. Verhey. 2009. Mammalian Kinesin-3 motors are dimeric in vivo and move by processive motility upon release of autoinhibition. *PLoS Biol.* 7:e72. https://doi.org/10.1371/journal.pbio.1000072

Hendricks, A.G., E. Perlson, J.L. Ross, H.W. Schroeder III, M. Tokito, and E.L.F. Holzbaur. 2010. Motor coordination via a tug-of-war mechanism drives bidirectional vesicle transport. *Curr. Biol.* 20:697–702. https://doi.org/10.1016/j.cub.2010.02.058

Hirokawa, N., and Y. Noda. 2008. Intracellular transport and kinesin superfamily proteins, KIFs: structure, function, and dynamics. *Physiol. Rev.* 88:1089–1118. https://doi.org/10.1152/physrev.00023.2007

Hoogenraad, C.C., A. Akhmanova, S.A. Howell, B.R. Dortland, C.I. De Zeeuw, R. Willemsen, P. Visser, F. Grosveld, and N. Galjart. 2001. Mammalian Golgi-associated Bicaudal-D2 functions in the dynein-dynactin pathway by interacting with these complexes. *EMBO J.* 20:4041–4054. https://doi.org/10.1093/emboj/20.15.4041

Hornbeck, P.V., B. Zhang, B. Murray, J.M. Kornhauser, V. Latham, and E. Skrzypek. 2015. PhosphoSitePlus, 2014: mutations, PTMs and recalibrations. *Nucleic Acids Res.* 43(D1):D512–D520. https://doi.org/10.1093/nar/gku1267

Kamal, A., G.B. Stokin, Z. Yang, C.H. Xia, and L.S. Goldstein. 2000. Axonal transport of amyloid precursor protein is mediated by direct binding to the kinesin light chain subunit of kinesin-I. *Neuron.* 28:449–459. https://doi.org/10.1016/S0896-6273(00)00124-0

Kim, D.I., K.C. Birendra, W. Zhu, K. Motamedchaboki, V. Doye, and K.J. Roux. 2014. Probing nuclear pore complex architecture with proximity-dependent biotinylation. *Proc. Natl. Acad. Sci. USA.* 111:E2453–E2461. https://doi.org/10.1073/pnas.1406459111

Kopp, P., R. Lammers, M. Aepfelbacher, G. Woehlke, T. Rudel, N. Machuy, W. Steffen, and S. Linder. 2006. The kinesin KIF1C and microtubule plus ends regulate podosome dynamics in macrophages. *Mol. Biol. Cell.* 17:2811–2823. https://doi.org/10.1091/mbc.e05-11-1010

Lee, I.-G., M.A. Olenick, M. Boczkowska, C. Franzini-Armstrong, E.L.F. Holzbaur, and R. Dominguez. 2018. A conserved interaction of the dynein light intermediate chain with dynein-dynactin effectors necessary for processivity. *Nat. Commun.* 9:986. https://doi.org/10.1038/s41467-018-03412-8

Lee, P.L., M.B. Ohlson, and S.R. Pfeffer. 2015. Rab6 regulation of the kinesin family KIF1C motor domain contributes to Golgi tethering. *eLife.* 4:917. https://doi.org/10.7554/eLife.06029

Li, S.H., C.A. Gutekunst, S.M. Hersch, and X.J. Li. 1998. Interaction of huntingtin-associated protein with dynactin P150Glued. *J. Neurosci.* 18:1261–1269. https://doi.org/10.1523/JNEUROSCI.18-04-01261.1998

Lipka, J., L.C. Kapitein, J. Jaworski, and C.C. Hoogenraad. 2016. Microtubule-binding protein doublecortin-like kinase 1 (DCLK1) guides kinesin-3-mediated cargo transport to dendrites. *EMBO J.* 35:302–318. https://doi.org/10.15252/embj.201592929

Maday, S., K.E. Wallace, and E.L.F. Holzbaur. 2012. Autophagosomes initiate distally and mature during transport toward the cell soma in primary neurons. *J. Cell Biol.* 196:407–417. https://doi.org/10.1083/jcb.201106120

McKenney, R.J., W. Huynh, M.E. Tanenbaum, G. Bhabha, and R.D. Vale. 2014. Activation of cytoplasmic dynein motility by dynactin-cargo adapter complexes. *Science.* 345:337–341. https://doi.org/10.1126/science.1254198

McWilliam, H., W. Li, M. Uludag, S. Squizzato, Y.M. Park, N. Buso, A.P. Cowley, and R. Lopez. 2013. Analysis Tool Web Services from the EMBL-EBI. *Nucleic Acids Res.* 41(W1):W597-600. https://doi.org/10.1093/nar/gkt376

Miki, H., Y. Okada, and N. Hirokawa. 2005. Analysis of the kinesin superfamily: insights into structure and function. *Trends Cell Biol.* 15:467–476. https://doi.org/10.1016/j.tcb.2005.07.006

Moore, J.K., M.D. Stuchell-Brereton, and J.A. Cooper. 2009. Function of dynein in budding yeast: mitotic spindle positioning in a polarized cell. *Cell Motil. Cytoskeleton.* 66:546–555. https://doi.org/10.1002/cm.20364

Novarino, G., A.G. Fenstermaker, M.S. Zaki, M. Hofree, J.L. Silhavy, A.D. Heiberg, M. Abdellateef, B. Rosti, E. Scott, L. Mansour, et al. 2014. Exome sequencing links corticospinal motor neuron disease to common neurodegenerative disorders. *Science.* 343:506–511. https://doi.org/10.1126/science.1247363

Olenick, M.A., and E.L.F. Holzbaur. 2019. Dynein activators and adaptors at a glance. *J. Cell Sci.* 132:jcs227132. https://doi.org/10.1242/jcs.227132

Olenick, M.A., M. Tokito, M. Boczkowska, R. Dominguez, and E.L.F. Holzbaur. 2016. Hook Adaptors Induce Unidirectional Processive Motility by Enhancing the Dynein-Dynactin Interaction. *J. Biol. Chem.* 291: 18239–18251. https://doi.org/10.1074/jbc.M116.738211

Ran, F.A., P.D. Hsu, J. Wright, V. Agarwala, D.A. Scott, and F. Zhang. 2013. Genome engineering using the CRISPR-Cas9 system. *Nat. Protoc.* 8: 2281–2308. https://doi.org/10.1038/nprot.2013.143

Reck-Peterson, S.L., W.B. Redwine, R.D. Vale, and A.P. Carter. 2018. The cytoplasmic dynein transport machinery and its many cargoes. *Nat. Rev. Mol. Cell Biol.* 19:382–398. https://doi.org/10.1038/s41580-018-0004-3

Redwine, W.B., M.E. DeSantis, I. Hollyer, Z.M. Htet, P.T. Tran, S.K. Swanson, L. Florens, M.P. Washburn, and S.L. Reck-Peterson. 2017. The human cytoplasmic dynein interactome reveals novel activators of motility. *eLife.* 6:e28257. https://doi.org/10.7554/eLife.28257

Roberts, A.J., B.S. Goodman, and S.L. Reck-Peterson. 2014. Reconstitution of dynein transport to the microtubule plus end by kinesin. *eLife.* 3:e02641. https://doi.org/10.7554/eLife.02641

Rogers, K.R., S. Weiss, I. Crevel, P.J. Brophy, M. Geeves, and R. Cross. 2001. KIF1D is a fast non-processive kinesin that demonstrates novel K-loop-dependent mechanochemistry. *EMBO J.* 20:5101–5113. https://doi.org/10.1093/emboj/20.18.5101

Rogers, S.L., I.S. Tint, P.C. Fanapour, and V.I. Gelfand. 1997. Regulated bidirectional motility of melanophore pigment granules along microtubules in vitro. *Proc. Natl. Acad. Sci. USA.* 94:3720–3725. https://doi.org/10.1073/pnas.94.8.3720

Roux, K.J., D.I. Kim, M. Raida, and B. Burke. 2012. A promiscuous biotin ligase fusion protein identifies proximal and interacting proteins in mammalian cells. *J. Cell Biol.* 196:801–810. https://doi.org/10.1083/jcb.201112098

Salogiannis, J., M.J. Egan, and S.L. Reck-Peterson. 2016. Peroxisomes move by hitchhiking on early endosomes using the novel linker protein PxdA. *J. Cell Biol.* 212:289–296. https://doi.org/10.1083/jcb.201512020

Schlager, M.A., L.C. Kapitein, I. Grigoriev, G.M. Burzynski, P.S. Wulf, N. Keijzer, E. de Graaff, M. Fukuda, I.T. Shepherd, A. Akhmanova, and C.C. Hoogenraad. 2010. Pericentrosomal targeting of Rab6 secretory vesicles by Bicaudal-D-related protein 1 (BICDR-1) regulates neuritogenesis. *EMBO J.* 29:1637–1651. https://doi.org/10.1038/emboj.2010.51

Schlager, M.A., H.T. Hoang, L. Urnavicius, S.L. Bullock, and A.P. Carter. 2014. In vitro reconstitution of a highly processive recombinant human dynein complex. *EMBO J.* 33:1855–1868. https://doi.org/10.15252/embj.201488792

Schroeder, C.M., and R.D. Vale. 2016. Assembly and activation of dynein-dynactin by the cargo adaptor protein Hook3. *J. Cell Biol.* 214:309–318. https://doi.org/10.1083/jcb.201604002

Siddiqui, N., A.J. Zwetsloot, A. Bachmann, D. Roth, H. Hussain, J. Brandt, I. Kaverina, and A. Straube. 2019. PTPN21 and Hook3 relieve KIF1C autoinhibition and activate intracellular transport. *Nat. Commun.* 10:2693. https://doi.org/10.1038/s41467-019-10644-9

Sowa, M.E., E.J. Bennett, S.P. Gygi, and J.W. Harper. 2009. Defining the human deubiquitinating enzyme interaction landscape. *Cell.* 138: 389–403. https://doi.org/10.1016/j.cell.2009.04.042

Splinter, D., M.E. Tanenbaum, A. Lindqvist, D. Jaarsma, A. Flotho, K.L. Yu, I. Grigoriev, D. Engelsma, E.D. Haasdijk, N. Keijzer, et al. 2010. Bicaudal D2, dynein, and kinesin-1 associate with nuclear pore complexes and regulate centrosome and nuclear positioning during mitotic entry. *PLoS Biol.* 8:e1000350. https://doi.org/10.1371/journal.pbio.1000350

Stock, M.F., J. Guerrero, B. Cobb, C.T. Eggers, T.G. Huang, X. Li, and D.D. Hackney. 1999. Formation of the compact conformer of kinesin requires a COOH-terminal heavy chain domain and inhibits microtubule-stimulated ATPase activity. *J. Biol. Chem.* 274:14617–14623. https://doi.org/10.1074/jbc.274.21.14617

Stuurman, N., M. Häner, B. Sasse, W. Hübner, B. Suter, and U. Aebi. 1999. Interactions between coiled-coil proteins: Drosophila lamin Dm0 binds to the bicaudal-D protein. *Eur. J. Cell Biol.* 78:278–287. https://doi.org/10.1016/S0171-9335(99)80061-2

Theisen, U., E. Straube, and A. Straube. 2012. Directional persistence of migrating cells requires Kif1C-mediated stabilization of trailing adhesions. *Dev. Cell.* 23:1153–1166. https://doi.org/10.1016/j.devcel.2012.11.005

Twelvetrees, A.E., E.Y. Yuen, I.L. Arancibia-Carcamo, A.F. MacAskill, P. Rostaing, M.J. Lumb, S. Humbert, A. Triller, F. Saudou, Z. Yan, and J.T. Kittler. 2010. Delivery of GABAARs to synapses is mediated by HAP1-KIF5 and disrupted by mutant huntingtin. *Neuron.* 65:53–65. https://doi.org/10.1016/j.neuron.2009.12.007

Twelvetrees, A.E., S. Pernigo, A. Sanger, P. Guedes-Dias, G. Schiavo, R.A. Steiner, M.P. Dodding, and E.L.F. Holzbaur. 2016. The Dynamic Localization of Cytoplasmic Dynein in Neurons Is Driven by Kinesin-1. *Neuron.* 90:1000–1015. https://doi.org/10.1016/j.neuron.2016.04.046

Urnavicius, L., K. Zhang, A.G. Diamant, C. Motz, M.A. Schlager, M. Yu, N.A. Patel, C.V. Robinson, and A.P. Carter. 2015. The structure of the dynactin complex and its interaction with dynein. *Science.* 347:1441–1446. https://doi.org/10.1126/science.aaa4080

Vale, R.D. 2003. The molecular motor toolbox for intracellular transport. *Cell.* 112:467–480. https://doi.org/10.1016/S0092-8674(03)00111-9

van Spronsen, M., M. Mikhaylova, J. Lipka, M.A. Schlager, D.J. van den Heuvel, M. Kuijpers, P.S. Wulf, N. Keijzer, J. Demmers, L.C. Kapitein, et al. 2013. TRAK/Milton motor-adaptor proteins steer mitochondrial trafficking to axons and dendrites. *Neuron.* 77:485–502. https://doi.org/10.1016/j.neuron.2012.11.027

Waterman-Storer, C.M. 2001. Microtubule/organelle motility assays. *Curr Protoc Cell Biol.* Chapter 13:Unit 13.1.

Wedlich-Söldner, R., A. Straube, M.W. Friedrich, and G. Steinberg. 2002. A balance of KIF1A-like kinesin and dynein organizes early endosomes in the fungus Ustilago maydis. *EMBO J.* 21:2946–2957. https://doi.org/10.1093/emboj/cdf296

Xu, L., M.E. Sowa, J. Chen, X. Li, S.P. Gygi, and J.W. Harper. 2008. An FTS/Hook/p107(FHIP) complex interacts with and promotes endosomal clustering by the homotypic vacuolar protein sorting complex. *Mol. Biol. Cell.* 19:5059–5071. https://doi.org/10.1091/mbc.e08-05-0473

Yamada, K.H., T. Hanada, and A.H. Chishti. 2007. The effector domain of human Dlg tumor suppressor acts as a switch that relieves auto-inhibition of kinesin-3 motor GAKIN/KIF13B. *Biochemistry.* 46: 10039–10045. https://doi.org/10.1021/bi701169w

Yao, X., X. Wang, and X. Xiang. 2014. FHIP and FTS proteins are critical for dynein-mediated transport of early endosomes in Aspergillus. *Mol. Biol. Cell.* 25:2181–2189. https://doi.org/10.1091/mbc.e14-04-0873

Zhang, J., S. Li, R. Fischer, and X. Xiang. 2003. Accumulation of cytoplasmic dynein and dynactin at microtubule plus ends in Aspergillus nidulans is kinesin dependent. *Mol. Biol. Cell.* 14:1479–1488. https://doi.org/10.1091/mbc.e02-08-0516

Zhang, J., R. Qiu, H.N. Arst Jr., M.A. Peñalva, and X. Xiang. 2014. HookA is a novel dynein-early endosome linker critical for cargo movement in vivo. *J. Cell Biol.* 204:1009–1026. https://doi.org/10.1083/jcb.201308009

Zhang, Y., Z. Wen, M.P. Washburn, and L. Florens. 2010. Refinements to label free proteome quantitation: how to deal with peptides shared by multiple proteins. *Anal. Chem.* 82:2272–2281. https://doi.org/10.1021/ac9023999